Volume 7 JANUARY, 1936 Number 1

PHYSICS

A Journal of General and Applied Physics

Stress Analysis by X-Ray Diffraction

C. S. BARRETT AND M. GENSAMER, *Metals Research Laboratory, Carnegie Institute of Technology, Pittsburgh*

(Received September 11, 1935)

A mathematical analysis is presented for the problem of determining stresses in a metal by x-ray diffraction. The treatment is a general one, including as special cases the various methods for the determination of uniaxial stresses or the *sum* of two principal stresses in the plane of the metal surface. The analysis is extended to the problem of determining the two principal surface stresses *individually*. Methods are proposed by which these stresses may be determined with an accuracy calculated to be of the order of 1300 lbs./in.^{2} for iron and 320 lbs./in.^{2} for duralumin, under the best conditions. Camera design, exposure technique, and the applicability of the method to practical problems are discussed.

THE measurement of stresses by the diffraction of monochromatic x-rays has passed from the unpromising stage when Lester and Aborn[1] in 1925 showed that such measurement was possible in thin strips of steel if extreme care were taken, to a stage where it is now ready for application to a variety of practical problems. In fact some metallurgical applications have already been made.[2] The important advances in technique which made this possible were the development of the back reflection camera[3, 4] and the use of suitable wave-lengths to provide diffraction at more favorable angles.[5]

Careful study of these developments has convinced us that the full possibilities of the method have not yet been put to use. In previous methods the diffraction rings from a stressed metal have been assumed to be (or made to be) circles; measurement of the diameter of these circles gives the *sum* of the two principal stresses in the plane of the surface, not the magnitude of the individual stresses (unless the stress system is uniaxial). If, however, the diffraction rings are measured as noncircular rings it is possible from their maximum and minimum diameters to calculate the maximum shear stress and the *individual* principal stresses in the plane of the surface. With appropriate arrangements of apparatus for this purpose it appears possible to achieve an accuracy in stress measurement sufficient to make the method of practical value.

In the following section we present a general analysis of the problem, and show that it should be possible to determine the magnitude of the maximum shear stress and the individual magnitudes and directions of the two principal stresses in the plane of the surface. The former methods will then be presented as special cases of this general analysis; the best operating conditions will be defined, and an evaluation will be made of the practical possibilities of the method.

The General Analysis

Under homogeneous elastic deformation, a spherical element of volume in an isotropic solid is deformed into an ellipsoid. Let us choose a rectangular coordinate system such that the X and Y axes lie in the plane of the surface of the specimen and parallel to the major and minor axes of this ellipsoid of deformation. The strain ϵ

[1] H. H. Lester and R. H. Aborn, Army Ordnance **6**, 120, 200, 283, 363 (1925–1926).
[2] H. Möller and I. Barbers, Mitt. Kaiser Wilhelm Institut für Eisenforschung **16**, Abhandlung 247, 21 (1934).
[3] G. Sachs and J. Weerts, Zeits. f. Physik **64**, 344 (1930).
[4] F. Wever and H. Möller, Archiv f. d. Eisenhüttenwesen **5**, 215 (1931).
[5] A. E. van Arkel and W. G. Burgers, Zeits. f. Metallkunde **23**, 149 (1931).

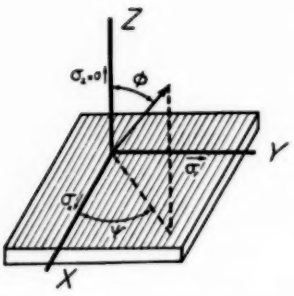

FIG. 1. Orientation of axes.

in any direction will then be related to the principal strains ϵ_X, ϵ_Y and ϵ_Z along the X, Y, and Z axes, respectively, by the approximate equation

$$\epsilon = a_X^2\epsilon_X + a_Y^2\epsilon_Y + a_Z^2\epsilon_Z, \tag{1}$$

where a_X, a_Y and a_Z are the direction cosines of the chosen direction and where the principal strains will be related to the principal stresses σ_X, σ_Y and σ_Z by

$$\begin{aligned}\epsilon_X &= (1/E)[\sigma_X - \nu(\sigma_Y+\sigma_Z)],\\ \epsilon_Y &= (1/E)[\sigma_Y - \nu(\sigma_X+\sigma_Z)],\\ \epsilon_Z &= (1/E)[\sigma_Z - \nu(\sigma_X+\sigma_Y)].\end{aligned} \tag{2}$$

In these expressions E is Young's modulus, ν is Poisson's ratio. The direction cosines may be expressed in terms of the angle to the Z axis, ϕ, and the azimuth angle about the Z axis, ψ (Fig. 1) by the relations

$$a_X = \sin\phi\cos\psi;\ a_Y = \sin\phi\sin\psi;\ a_Z = \cos\phi. \tag{3}$$

In layers near the surface of the specimen, where all x-ray reflection takes place in the case of metals, the stress normal to the surface is zero and using expressions (1), (2), and (3) we may write

$$\begin{aligned}\epsilon = (1/E)\{&[\sin^2\phi\cos^2\psi\\ &-\nu(\sin^2\phi\sin^2\psi+\cos^2\phi)]\sigma_X\\ &+[\sin^2\phi\sin^2\psi-\nu(\sin^2\phi\cos^2\psi+\cos^2\phi)]\sigma_Y\}.\end{aligned} \tag{4}$$

If we measure this strain for a constant angle ϕ and two different values of ψ, say for $\psi=0°$ and $\psi=90°$, we may calculate the principal stresses in the stressed material. By Eq. (4)

$$\epsilon_{\psi=0°} = (1/E)[(\sin^2\phi - \nu\cos^2\phi)\sigma_X - \nu\sigma_Y] \tag{5}$$

and

$$\epsilon_{\psi=90°} = (1/E)[(\sin^2\phi - \nu\cos^2\phi)\sigma_Y - \nu\sigma_X]. \tag{6}$$

The sum and difference of the principal stresses will therefore be given by

$$\sigma_X+\sigma_Y = (\epsilon_{\psi=0°}+\epsilon_{\psi=90°})E/[(1+\nu)\sin^2\phi - 2\nu] \tag{7}$$

and

$$\sigma_X-\sigma_Y = (\epsilon_{\psi=0°}-\epsilon_{\psi=90°})E/(1+\nu)\sin^2\phi \tag{8}$$

on the assumption that $\phi_{\psi=0°}$ is nearly equal to $\phi_{\psi=90°}$; this assumption is valid for the small changes in ϕ encountered in x-ray measurement of stress.

The sum of the expressions (7) and (8) will then give σ_X, while the difference will give σ_Y, in terms of known or measurable quantities. The values of E and ν are ordinarily known for the material. The ϵ terms and ϕ may be determined by the diffraction of a collimated beam of monochromatic x-rays,—by an x-ray extensometer, one might say, in which the distance between atomic planes serves as the gauge length. Under stress an interplanar distance d_0 changes to a distance d; ϵ is the strain normal to the crystallographic plane, and may be expressed by $\epsilon=(d-d_0)/d_0$ (later referred to as $\Delta d/d$).

X-rays of a given wave-length λ will reflect from those grains in a polycrystalline aggregate for which the possible reflecting planes fulfill the conditions of the Bragg law, $n\lambda=2d\sin\theta$. Changes in the interplanar distance, d, are determined by measuring changes in θ, the angle between the reflecting plane and the incident ray. Thus ϵ may be calculated from changes in θ. By measuring θ in the planes $\psi=0°$ and $\phi=90°$ (the planes containing the incident x-ray beam and the directions of each of the principal stresses) $\epsilon_{\psi=0°}$ and $\epsilon_{\psi=90°}$ are obtained for a particular value of ϕ, from which σ_X and σ_Y may be calculated by the use of Eqs. (7) and (8). The directions of the principal stresses may be determined, if they are not previously known, by locating the direction in which ϵ reaches a maximum or a minimum for any given value of ϕ. Eqs. (7) and (8) and those in the following section may, of course, be written with the ϵ terms replaced by functions of the angle θ; this has been done in the second section below.

Special Cases

The methods previously published for the analysis of stress by back reflection photograms may be shown to be special cases of the general theory just given.

The early stress measurements by Lester and Aborn[1] were made with x-rays penetrating a strip of steel loaded uniaxially. In our notation, their stress σ_X was applied along the X axis, the x-ray beam penetrated the strip approximately perpendicularly (along the Z axis), and the diffraction lines were measured in the $\psi=0°$ plane. It will be seen from Eq. (5) with $\sigma_Y=0$ that the stress in this case would be given by the relation[6]

$$\sigma_X=(E\cdot\epsilon_{\psi=0°})/(\sin^2\phi-\nu\cos^2\phi),$$

which may be written

$$\sigma_X=(E\cdot\epsilon_{\psi=0°})/[(1+\nu)\sin^2\phi-\nu]. \quad (9)$$

Sachs and Weerts[3] measured uniaxial stresses (assuming $\sigma_Y=\sigma_Z=0$) by means of a back reflection camera with a flat film mounted perpendicularly to the x-ray beam. Making use of the fact that $\epsilon_{\psi=0°}$ is approximately equal to $\epsilon_{\psi=90°}$ at small values of ϕ, they directed the beam along the Z axis of coordinates and rotated the film about this axis without causing an appreciable widening of the diffracted line; the result was a diffraction ring free from spots and irregularities. From the diameter of the circular diffraction rings thus produced one may calculate the average strain, $\epsilon_{av.}$, at the angle ϕ, and since it is a sufficiently accurate approximation to write $\epsilon_{av.}=\frac{1}{2}(\epsilon_{\psi=0°}+\epsilon_{\psi=90°})$ we may put this directly into Eq. (7) and with $\sigma_Y=0$ we obtain

$$\sigma_X=2\epsilon_{av.}E/[(1+\nu)\sin^2\phi-2\nu]. \quad (10)$$

The more important *biaxial* case discussed by Wever and Möller[4] is also covered by Eq. (7). If the film in a back reflection camera is rotated, as in the previous case, about the beam with the beam normal to the specimen surface and if a wave-length is chosen such that some crystallographic plane diffracts the x-ray beam very nearly in the reverse direction, then ϕ is small, $\sin^2\phi$ is negligible, and (7) reduces to

$$\sigma_X+\sigma_Y=-\epsilon_{av.}E/\nu. \quad (11)$$

Optimum Conditions for Operation

From the foregoing expressions one may readily show the conditions most favorable to x-ray determinations of stress and strain. A differentiation of the Bragg law $n\lambda=2d\sin\theta$ gives $\partial\theta/\partial d=-1/d\tan\theta$, and since $\Delta\theta=(\partial\theta/\partial d)\Delta d$ when $\Delta\theta$ is small, as it is with elastic strain, we may write $\Delta\theta=-(\Delta d/d)\tan\theta$, or

$$\Delta\theta=-\epsilon\tan\theta. \quad (12)$$

This shows that a given strain ϵ will produce a maximum change in diffraction angle when θ approaches 90° as closely as experimental conditions will permit.

Lester and Aborn's forward reflection experiment, while it utilized as reflecting planes those which underwent the maximum change in interplanar distance, was handicapped by the low sensitivity of the diffraction angle to strain in the neighborhood of $\theta=0°$. The relative importance of these two factors for their experiment may be seen from Eq. (9) which, combined with (12), becomes

$$\Delta\theta=-(\sigma_X/E)[(1+\nu)\sin^2\phi-\nu]\tan\theta. \quad (13)$$

It will be noted that $\Delta\theta$, the shift in diffraction angle under stress, is zero both at $\theta=0°$ and at the angle ϕ for which $\sin^2\phi=\nu/(1+\nu)\cong 0.32/1.32$, an angle of about 30°; but both these points are outside the limits used in their experiments.

The change in diffraction angle for Sachs and Weerts' back reflection method may be derived from expressions (10) and (12) in the form

$$\Delta\theta_{av.}=-(\sigma_X/2E)[(1+\nu)\sin^2\phi-2\nu]\tan\theta. \quad (14)$$

Large angles of diffraction are used because this approaches a maximum as θ approaches 90°. Zero sensitivity occurs in this case when $\sin^2\phi=2\nu/(1+\nu)$ which is in the neighborhood of $\phi=44°$, a region not used in the normal back reflection technique. (Sachs and Weerts rotated their photographic plate and thus averaged θ for

[6] The method of calculation used by Lester and Aborn could be written in terms of our notation as

$$\sigma_X=E\cdot\epsilon_{\psi=0°}/\sin\phi.$$

This is a rather rough approximation to our Eq. (9); the error in this expression is 2.5 percent for the Mo $K\alpha$ (110) reflection from steel at $\phi=80°$ but increases with the reflections from planes of higher indices and reaches 25 percent for their outermost line, the (321) reflection at $\phi=62°$.

all values of ψ, which Lester and Aborn did not do; this accounts for the difference in the zero sensitivity value of ϕ for the two cases.)

The corresponding equation for Wever and Möller's case, obtained from Eqs. (11) and (12), is

$$\Delta\theta_{\text{av.}}=(\nu/E)(\sigma_X+\sigma_Y)\tan\theta, \qquad (15)$$

and again the use of the largest possible value of θ is indicated. This is an approximation to

$$\Delta\theta_{\psi=0^\circ}+\Delta\theta_{\psi=90^\circ}$$
$$=-(1/E)[(1+\nu)\sin^2\phi-2\nu](\sigma_X+\sigma_Y)\tan\theta \quad (16)$$

derived from Eqs. (7) and (12).

While measurements at the largest possible θ values are most desirable for the determination of uniaxial stresses or the sum of the principal stresses, they are unsuited, in the case of the x-ray beam incident normally on the surface, for measurements of the difference (or the ratio) of the two principal stresses, and for determining the principal stresses individually as proposed in this paper. The difference in the diffraction shift in the $\psi=0^\circ$ and $\psi=90^\circ$ planes may be derived from Eqs. (8) and (12), and is

$$\Delta\theta_{\psi=0^\circ}-\Delta\theta_{\psi=90^\circ}$$
$$=-(1/E)(\sigma_X-\sigma_Y)(1+\nu)\sin^2\phi\tan\theta. \quad (17)$$

For the case of the incident beam falling perpendicularly upon the surface of the specimen, so that $\tan\theta=\cot\phi$, this reduces to

$$\Delta\theta_{\psi=0^\circ}-\Delta\theta_{\psi=90^\circ}$$
$$=-(1/2E)(\sigma_X-\sigma_Y)(1+\nu)\sin 2\phi, \quad (18)$$

which increases from zero at $\phi=0^\circ$ to a maximum at $\phi=45^\circ$. If one were able, therefore, to measure the diffraction angle with equal accuracy throughout the range $\phi=0^\circ$ to $\phi=45^\circ$ ($2\theta=90^\circ$), the best technique, limiting the discussion to the case of the x-ray beam falling perpendicularly upon the surface, would be to determine $(\sigma_X+\sigma_Y)$ in the neighborhood of $\theta=90^\circ$ ($\phi=0^\circ$), and $(\sigma_X-\sigma_Y)$ in the neighborhood of $\theta=45^\circ$ ($2\theta=90^\circ$, and $\phi=45^\circ$). Either of these quantities might, of cuorse, be determined from several different diffraction lines at different angles.

In the more general case of an x-ray beam falling obliquely upon the surface of the specimen,

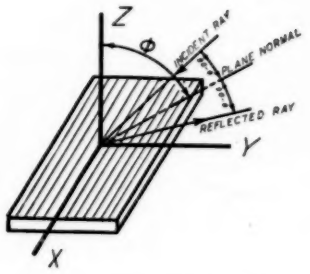

FIG. 2. Case of oblique incidence.

it will be seen from Eq. (17) that the most favorable arrangement for measuring the difference in stresses would be one which made both θ and ϕ nearly 90° (see Fig. 2). Using Co $K\alpha$ radiation directed obliquely toward the surface of a steel specimen, θ could be made as large as about 80° 45′ and ϕ probably about 70°; this would require that either the incident beam or the reflected ray make an angle of about 10° with the surface. The relatively large diffraction line shifts under these conditions invite an attempt to overcome the difficulties that would be encountered.

THE PROBABLE ERRORS IN STRESS DETERMINATION

It is of considerable importance to know exactly what accuracy may be expected in the measurement of the individual principal stresses σ_X and σ_Y and in their difference $(\sigma_X-\sigma_Y)$, by the method proposed in this paper, for upon this knowledge must rest the decision as to whether or not the method should receive active experimental development.

Eqs. (16) and (17) may be written in the form

$$(\sigma_X+\sigma_Y)=-E\frac{\cot\theta}{[(1+\nu)\sin^2\phi-2\nu]}$$
$$\times(\Delta\theta_{\psi=0^\circ}+\Delta\theta_{\psi=90^\circ}\pm\sqrt{2}r) \quad (19)$$

and

$$(\sigma_X-\sigma_Y)=-E\frac{\cot\theta}{(1+\nu)\sin^2\phi}$$
$$\times(\Delta\theta_{\psi=0^\circ}-\Delta\theta_{\psi=90^\circ}\pm\sqrt{2}r) \quad (20)$$

if it is assumed that the probable errors in measuring $\Delta\theta_{\psi=0^\circ}$ and $\Delta\theta_{\psi=90^\circ}$ are the same and equal

to r radians. The corresponding expression for Wever and Möller's Eq. (15) is

$$(\sigma_X+\sigma_Y)=(E/\nu)\cot\theta(\Delta\theta_{\text{av.}}\pm r). \qquad (21)$$

Möller and Barbers[2] consider that an accuracy of 2 kg/mm² (2800 lbs./in.²) in $(\sigma_X+\sigma_Y)$ may be readily obtained with the best of present-day back reflection technique when the specimen is iron. We shall adopt this figure as the probable error in stress measurement under their conditions, i.e., when using the (310) reflection of Co $K\alpha$ radiation at $\theta=80°\ 45'$, with the x-ray beam normal to the surface. The probable error in angle corresponding to this, calculated from Eq. (21), is

$$r=2800\times(0.32/(30\times10^6))\times6.140=1.83\times10^{-4}$$

radians (or 38 seconds). Now if an attempt were made to determine $(\sigma_X-\sigma_Y)$ under the same conditions and with the same probable error in angle measurement, the difference of stresses according to Eq. (20) would be

$$(\sigma_X-\sigma_Y)=\frac{2E}{1+\nu}\frac{1}{\sin 2\theta}(\Delta\theta_{\psi=0°}-\Delta\theta_{\psi=90°}\pm\sqrt{2}r) \qquad (22)$$

and the probable error would be

$$\frac{2\times30\times10^6}{1.32}\times\frac{1}{0.317}\times\sqrt{2}\times1.83\times10^{-4}$$

$$=37{,}000\text{ lbs./in.}^2.$$

The individual stresses, obtained by addition and subtraction of Eqs. (21) and (22) would have a probable error of

$$\tfrac{1}{2}[(37{,}000)^2+(2800)^2]^{\frac{1}{2}}=18{,}600\text{ lbs./in.}^2,$$

which is probably too great to make the data of practical use.

It was shown in the preceding section that with the x-ray beam falling perpendicularly upon the specimen the best range in which to apply the formulas for $(\sigma_X-\sigma_Y)$ is in the range near $\phi=45°$; here the probable error in $(\sigma_X-\sigma_Y)$ corresponding to our assumed error in angle has the value, obtained from (22),

$$[(2\times30\times10^6)/1.32]\times1\times\sqrt{2}\times1.83\times10^{-4}$$

$$=12{,}000\text{ lbs./in.}^2.$$

Since the maximum shear stress is given by $\frac{1}{2}(\sigma_X-\sigma_Y)$, the probable error in maximum shear stress will be about 6000 lbs./in.². Combining a measurement of $(\sigma_X-\sigma_Y)$ at $\phi=45°$ with a measurement of $(\sigma_X+\sigma_Y)$ at $\phi=9°\ 15'$ the error in σ_X and σ_Y individually is

$$\tfrac{1}{2}[(12{,}000)^2+(2800)^2]^{\frac{1}{2}}=6200\text{ lbs./in.}^2.$$

In the more general case of an oblique incident beam, using $\phi=70°$ and $\theta=80°\ 45'$ (Co $K\alpha$ (310) reflection), Eq. (19) yields for the sum $(\sigma_X+\sigma_Y)$ an error of

$$\frac{30\times10^6\times0.163}{(1.32\times0.883)-0.64}\times\sqrt{2}\times1.83\times10^{-4}$$

$$=2400\text{ lbs./in.}^2$$

and for the difference $(\sigma_X-\sigma_Y)$, from Eq. (20),

$$\frac{30\times10^6}{1.32}\times\frac{0.163}{0.883}\times\sqrt{2}\times1.83\times10^{-4}=1100\text{ lbs./in.}^2.$$

The corresponding error in maximum shear stress would therefore be 600 lbs./in.², and the error in the individual principal stresses

$$\tfrac{1}{2}[(2400)^2+(1100)^2]^{\frac{1}{2}}=1300\text{ lbs./in.}^2.$$

For the sake of easy comparison these calculations were made assuming the same probable error in measurement of angle as in the case of normal incidence, though it is doubtful that this can be reached in practice.

The same type of calculations will now be carried through for specimens of duralumin. If we assume again the same error in angle measurement and if a beam of Cu $K\alpha$ radiation falls perpendicularly from the specimen and reflects from (511) and (333) planes at $\phi=7°$, Eq. (21) will predict the probable error as $(10^7/0.34)\times0.123\times1.83\times10^{-4}=660$ lbs./sq. in.,[7] while in the neighborhood of $\phi=45°$, the probable error in $(\sigma_X-\sigma_Y)$ would be 3900 lbs./in.², according to Eq. (18), and the maximum shear stress error would be about 2000 lbs./in.². Combining these

[7] This figure is much less than Sachs and Weerts' estimate of ±2kg/mm² (±2800 lbs./in.²) from an earlier study (1930) probably with less refined experimental technique than was used by Möller and Barbers four years later. While the width of the diffraction lines from duralumin may be somewhat greater than from iron and may thus lower the accuracy, the assumptions used in the above calculations are probably reasonable.

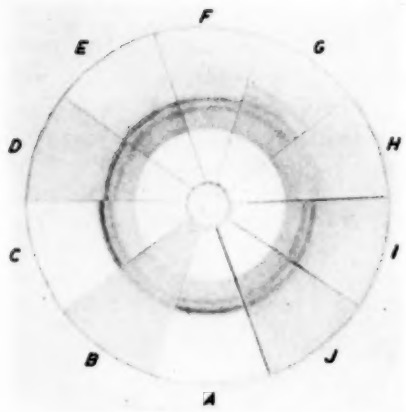

FIG. 3. Back reflection photograms of steels listed in Table I.*

TABLE I. *Relative line widths from different annealed steels.*

Type of Steel	Mark (Fig. 3)	Composition C	Mn	Si	Cr	Mo	Ni	Va	W	Line Width
Chrome-molybdenum	A	0.29	0.55	0.17	0.64	0.24				Normal
Chrome-nickel	B	0.3–0.6	0.3–0.4		0.5–0.6		1.0–1.2			"
Nickel	C	0.25	0.60	0.23			3.37			"
High carbon	D	1.05	0.30	0.35	0.07					"
Vanadium	E	0.9–1.0	0.4	0.3				0.20		"
Chromium	F	0.92	0.24	0.29	2.01					"
High speed	G	0.70	0.25		4.0			1.0	18.0	"
Cutlery stainless	H	0.3–0.4			12.–13.					Very wide
Low carbon Open-hearth	I									Normal
Low carbon Bessemer	J									"

exposures at the different ϕ values the error in σ_X and σ_Y would be 2000 lbs./in.^{2}.

On the other hand, if oblique incidence is used with $\phi=73°$ and $\theta=83°$ (the condition for the reflected ray leaving the surface at an angle of 10°), Eq. (19) would indicate an error of 580 lbs./in.^{2} in $(\sigma_X+\sigma_Y)$ and Eq. (20) an error of 260 lbs./in.^{2} in $(\sigma_X+\sigma_Y)$. The corresponding error in maximum shear stress would be 130 lbs./in.^{2}, and in the individual principal stresses 320 lbs./in.^{2}.

There has been some doubt that alloy steels and high carbon steels would give diffraction lines sharp enough to permit measurement with the high accuracy required for stress analysis. To test this point a series of back reflection photograms of various steels were prepared under identical conditions. The details are given in Table I, and the photograms are assembled in Fig. 3. All were packed in iron turnings, given an anneal of 2 hrs. at 900°C, cooled in the furnace, and then ground and etched. It was found that substantially the same diffraction line widths were obtained from low carbon steels and all the alloy steels except the cutlery stainless steel. Therefore the accuracy obtained by Wever and Möller, on which the calculations of this section are based, should be obtained as readily with about any structural steel in the annealed condition as with the annealed low carbon steels used by these investigators.

* The experimental conditions for these photograms were as follows: Both specimen and film rotated; the specimen-film distance was 8.00 cm; the x-ray beam was defined by a 1/2-mm pinhole placed on the axis of rotation of the film at the position to focus the Co $K\alpha$ reflection from (310) planes; a second pinhole limited the irradiated spot on the specimen to about 3 mm diam.

TECHNIQUE

A list of the desirable features of a camera for the determination of the principal stresses individually should be of value, for none of the usual cameras are suitable.

(1) A camera for operation with the beam falling perpendicularly on the specimen should provide films (or plates) to register diffraction lines for ϕ near 10° and also near 45° in two planes at right angles (the $\psi=0°$ and $\psi=90°$ planes). Additional measurements with other values of ϕ and ψ would be unnecessary, though possibly desirable. A camera for oblique incidence of the beam on the specimen should be designed to use reflections with ϕ as nearly 90° as possible. Two exposures would then be necessary, one with $\psi=0°$ and one with $\psi=90°$.

(2) The camera should provide collimating pinholes by which the beam could be made to strike a small, well-defined area on the metal specimen, and the pinholes should be so placed that the diffracted rays focus on the film; this requires that the smallest pinhole, the irradiated area on the specimen, and the diffracted line on the film all lie on the circumference of a circle.

(3) It should permit no uncertainty in the position of either films or specimen.

(4) A mechanism should be provided to oscillate the camera a few degrees about the x-ray beam as an axis thus producing smooth instead of spotty lines.

(5) The camera and its x-ray tube would be more useful if it were portable and could be moved to any position on the surface of a model or assembled structure.

We might sketch roughly some designs for such cameras. Perhaps the most obvious one for perpendicular incidence would place two films on cylinders having a common diameter and axes at

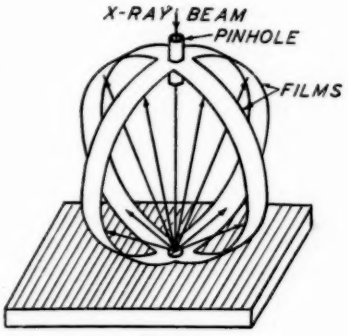

FIG. 4.

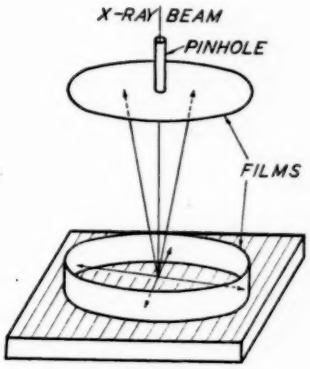

FIG. 5.

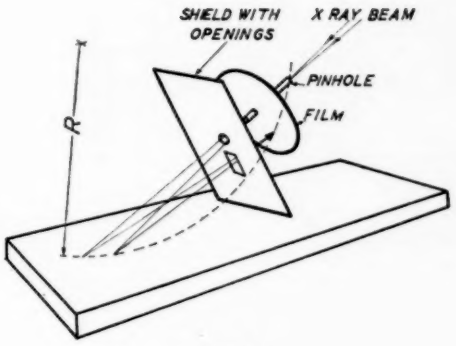

FIG. 6.

Suggested designs for diffraction cameras for biaxial stress determination.

90° to each other, as shown in Fig. 4. The x-ray beam would be directed along the common diameter by pinholes located at one end of the diameter and would strike the specimen surface at the other end. One film could then record the diffraction in the plane $\psi=0$ and the other in the plane $\psi=90°$, and diffraction lines would come to a focus on the films at all values of ϕ. Another possible arrangement would be as shown in Fig. 5, with one film (or plate) mounted perpendicular to the beam and drilled in the center to pass the beam through it, and with another film placed on a cylinder coaxial with the beam and near the surface of the specimen. The pinhole collimating the beam would be placed to focus one diffraction line on the flat film (a line near $\phi=0$) and another line on the cylindrical film (a line near $\phi=45°$).

For oblique incidence the simplest form would be a back reflection camera of the usual design with the smallest pinhole located at a suitable distance behind the flat film (or plate), as indicated in Fig. 6. This would bring only one reflection into focus on the film, but would have the advantage over other types that the diffracted ray would strike the film almost perpendicularly.

In all x-ray determinations of stress the surface of the specimen must be in a condition to give sharp lines.[8] If there are cold worked layers on the surface, left by machining, these must be etched away. Another important requirement is that the sample on which the stress-free measurement is made must be of exactly the same material as the stressed piece—in particular, both must have the same solid solution composition. Thus, for example, an x-ray study of the stresses in an age hardening aluminum alloy would be in error one if prepared a stress-free sample by an annealing treatment that caused either an additional precipitation from solid solution or a resolution of precipitated material, for in either case the solid solution matrix would have altered its lattice dimensions. An unstressed sample of a structural member could be obtained by carefully removing a cylinder with a hollow drill; the drilled hole could afterward be welded or filled with a rivet.

During the x-ray exposures the temperature must be kept constant to within a degree or better, and the temperature for the exposure of the unstressed sample must be the same as for the stressed sample or a correction must be applied for thermal expansion between these temperatures. If films are used instead of photographic plates, the shrinkage of the film must be considered. A satisfactory way of doing this would be to measure the distance between the diffraction lines and a set of standard lines diffracted from a thin layer of a powdered calibrating substance on the surface of the specimen. These measurements can probably be made most accurately by using a microphotometer.

DISCUSSION

The accuracy that can be reached in stress analysis by this method is not as high as one might desire, nor is the method simple and easy

[8] For a review of the subject of line width cf. C. S. Barrett, "Internal Stresses, Part III," Metals and Alloys **5**, 170 (1934).

in its application. Nevertheless, it possesses some advantages that may earn a place for it among the established methods of stress measurement. These may be summarized as follows:

(1) It applies to the surface stresses in a body which is under a three-dimensional stress system. No assumption is necessary that the stress remains constant throughout the thickness, as in photoelastic studies or in the method based on mechanical strain gauge measurements around a drilled hole.[9]

(2) It measures the internal stresses as well as those resulting from external loading.

(3) It should be applicable to a completed structure (a bridge, for example) during service without removal of the service load and without damage to the structure.

(4) It measures the difference in the principal stresses as well as the sum,—and failure under stress is more closely related to the difference than to the sum.

(5) Only a small area need be irradiated by the x-ray beam. It is thus applicable to problems where small gauge lengths are necessary, and in fact might enable stress concentrations to be mapped out on smaller models than are needed for mechanical strain gauge studies.

Lieutenant Robert H. Haskell, working at Watertown Arsenal and in collaboration with Professor John T. Norton, Professor Charles E. Fuller and Dr. H. H. Lester, saw the possibility of biaxial stress analysis by x-rays and worked out independently and simultaneously equations analogous to our Eqs. (4), (5) and (6).[10, 11] We are indebted to this group and to Mr. R. G. Sturm of the Aluminum Company of America for stimulating discussions of the paper.

Note added to proof: Our attention has been called to a paper by R. Glocker and E. Osswald[12] in which equations are developed similar to our Eqs. (1) to (8), and covering the problem of determining the direction as well as the magnitude of the principal stresses. From laboratory tests they conclude that with favorable technique the individual stresses can be determined with an accuracy equal to or greater than that which has been attained in the sum of the stresses by previous x-ray methods. It will be seen that this is in agreement with the conclusions of the present paper.

[9] J. Mather, Archiv f. d. Eisenhüttenwesen **6**, 277 (1933).

[10] Robert H. Haskell, Masters thesis, Massachusetts Institute of Technology, 1934.

[11] C. S. Barrett and M. Gensamer, Phys. Rev. **45**, 563A (1934).

[12] R. Glocker and E. Osswald, Zeits. f. tech. Physik **16**, 237–242 (1935).

Permeability of Compacted Powders

Determination of Average Pore Size

R. N. TRAXLER AND L. A. H. BAUM, *The Barber Asphalt Company, Maurer, N. J.*

(Received September 19, 1935)

With air as the diffusing medium a method and apparatus have been developed for measuring the permeability of compacted, unconsolidated powders. A formula is given for calculating the average pore diameter from the permeability and the percent of voids in the compacted powder. By establishing a simple relationship between the degree of packing, as measured by the percent voids, and the average individual pore diameter it is possible to calculate the pore size in a comminuted solid for any degree of compaction. When liquids (e.g., bitumen, sulfur, etc:) are stabilized by the addition of solid particles, the degree of packing of the particles and the dimensions of the films and masses of liquid separating them exert a profound influence on the consistency of the mixture. Thus, a knowledge of the average pore diameter of a powder as present in a solid-liquid system is of practical value. The influence of average particle size on average pore diameter was studied and data are presented for silica and slate powders.

INTRODUCTION

VALUES for the permeabilities of compacted pulverulent solids and estimations of the average size of the individual pores or capillaries present have many applications. Diffusion of gases and liquids through soil and comminuted minerals is of interest to the agriculturist, ceramist, geologist, ore treater, and engineer. As an example, the permeability of the materials used in hydraulic-fill dams has been studied by Terzaghi, Gilboy and others. In filtration problems the size of the individual pores in the filtering medium or build-up cake is of paramount importance. An optimum permeability and average interstitial pore size exists for char filters used in purifying sugar and other organic compounds. Average pore diameter is as important as the volume percent of voids in heat transfer problems incident to the operation of blast furnaces, limestone kilns, and in the applications of porous insulating materials.

The amount of voids in a compacted, comminuted solid is frequently adjusted by regulation of the particle size and distribution, but it is often overlooked that these changes, also, affect the dimensions of the average individual pore. When a powdered material is employed as a filler or stabilizing agent for a fluid the average thickness of the individual films or spaces between the solid particles, as distributed in the mixture, greatly influences the consistency and characteristics of the system.

In the design of mineral-filled bituminous materials, which are to be used for paving, roofing or industrial applications, the consistency of the finished material must be considered. Therefore, the apparatus and method described below were developed for measuring experimentally the permeabilities to air of fine, compacted, pulverulent solids. From the values so obtained the average pore sizes were then calculated.

THEORY

Bartell and Osterhof[1] give an excellent review of several methods for estimating pore radius. Their discussion of the subject was most helpful, as was the work of Wyckoff, Botset, Muskat and Reed,[2] and others on permeability. The measurement of the permeability to a gas (air) was selected as the method by means of which the average pore diameter of compacted powders could be estimated most rapidly and satisfactorily. Also, the necessary apparatus and technique were comparatively simple and good check determinations could be obtained. If a liquid is substituted for the gas, permeability values cannot be obtained at various degrees of packing because with such a diffusion medium rearrangements will occur in the compacted but unconsolidated powder. When a gas is passed through the compacted material a fixed state of packing can be maintained in the entire sample throughout the experiment.

[1] F. E. Bartell and H. J. Osterhof, J. Phys. Chem. **32**, 1553 (1928).

When a fluid under pressure is passed through a single capillary tube the size of the capillary can be obtained from the Hagen-Poiseuille formulation provided the pressure is not so high as to cause turbulence.

$$r^4 = 8\eta V' L/\pi pgt, \tag{1}$$

where r = the radius, in cm, of the capillary,
η = the viscosity, in poises, of the fluid passing through the tube,
V' = the volume, in cm³, of fluid passing in time "t," at the mean pressure.
L = length, in cm, of the capillary,
p = pressure drop, in g/cm², through the capillary,
g = gravitational constant = 980.6,
t = time of flow, in seconds, in which volume of fluid "V'" passes.

Now, in a compacted pulverulent material, which contains N capillaries of equal length and equal radius, the total volume V of all the capillaries is equal to NV'. By substituting V/N for V' and l, the length, in cm, of the column of compacted particles, for L in Eq. (1) we obtain

$$r^4 = 8\eta Vl/\pi Npgt. \tag{2}$$

In a compacted mass of solid particles the volume of voids is equal to the volume occupied by the compacted material multiplied by the percent of voids, and in a cross section through the mass, the area not filled by solid particles is equal to the volume of voids divided by the length of the column of compacted particles, or

$$A = v/l \tag{3}$$

where A = cross-sectional area, in cm², not filled by the solid particles,
v = volume, in cm³, of voids in the compacted powder.

If the cross-sectional area of the sample is represented by a, then

$$A = (a \times B)/100, \tag{4}$$

where B is the percent voids in the compacted powder. Also, if A is considered as made up of circular areas of radius, r, then

$$A = N\pi r^2, \tag{5}$$

where N = number of pores or voids,
r = average radius, in cm, of the pores.

Eq. (2) contains two unknown quantities, "r" and "N." By substituting $A/\pi r^2$ for N we eliminate N and have

$$r^4 = 8\eta Vl\pi r^2/\pi Apgt; \tag{6}$$

simplifying,

$$r = (8\eta Vl/Apgt)^{\frac{1}{4}}. \tag{7}$$

Since η, l, A and g are constant for a particular gas and a given sample, *the average individual pore radius in the sample can be found merely by varying p and measuring the corresponding values of V/t.*

Further, r may also be expressed in terms of permeability which has been defined quantitatively[2] as the volume of fluid of unit viscosity passing through in unit time, a unit cross section of the porous material under the influence of a unit pressure gradient, or

$$K = \eta \bar{q} l/a(P_1 - P_2), \tag{8}$$

where K = permeability,
$\bar{q}$ = corrected rate of flow, in cm³/sec.,
$= \frac{2 \text{ barometric pressure}}{P_1 + P_2} \times q$, where q = measured rate of flow,
P_1 = absolute upstream pressure, in g/cm²,
P_2 = absolute downstream pressure, in g/cm².

By substituting in Eq. (7) $\bar{q}$ for V/t, $P_1 - P_2$ for p, and for A its equivalent, $(a \times B)/100$, we obtain

$$r = \left(\frac{800}{g \times B} \cdot \frac{\eta \bar{q} l}{a(P_1 - P_2)} \right)^{\frac{1}{4}}; \tag{9}$$

further, substituting K from Eq. (8) and Eq. (9) we have

$$r = \left(\frac{800}{g \times B} \times K \right)^{\frac{1}{4}}. \tag{10}$$

Thus, if the void content of a compacted powder is known the average individual pore radius may be calculated from the permeability factor.

Apparatus and Method

Although considerable work had been done by various investigators, especially those interested in determining the permeabilities of oil sands,

[2] R. D. Wyckoff, H. G. Botset, M. Muskat and D. W. Reed, Rev. Sci. Inst. **4**, 394 (1933).

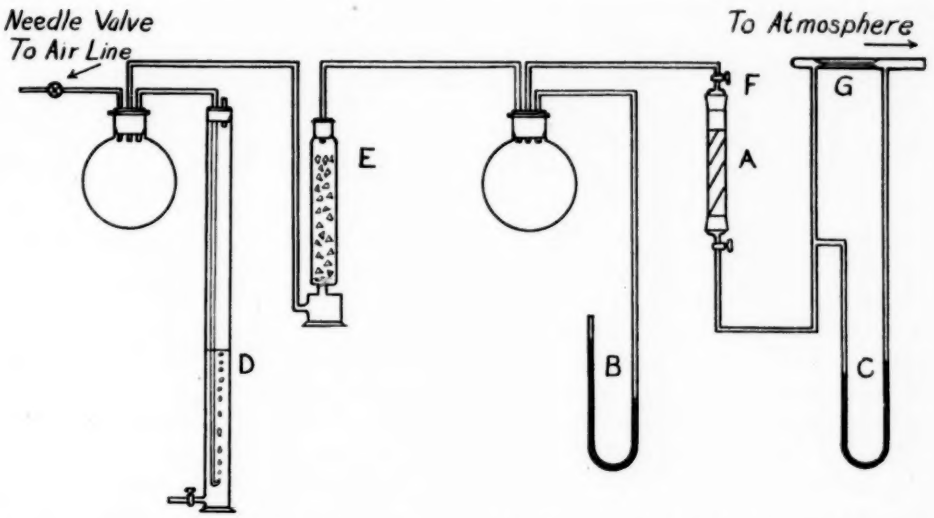

FIG. 1. Diagrammatic sketch of apparatus used for determining average pore diameter in compacted pulverulent material.

etc.,[3–8] numerous problems were encountered in the investigation of compacted, fine mineral powders which were not met with in coarse consolidated sands.

A diagram of the apparatus used is shown in Fig. 1. Cell, *A*, holds a column of compacted dust 15 to 20 cm long. *B* is the upstream manometer, while a flow meter, *C*, which measures the volume of air passing through the sample, also serves as a downstream manometer. The cell and flow meter are located in a wooden cabinet with a glass door. The temperature inside the cabinet is maintained constant within 0.5°C by means of a thermostatically operated electric heater, a cooling coil and an electric fan to circulate the air. Constant temperature must be maintained because expansion and contraction of the air in the cell and flow meter, because of changes in temperature, will create fluctuations in the recorded pressure. *D* is a pressure regulator less elaborate but similar to that designed by Bingham.[9] Air is delivered to the regulator under a pressure slightly greater than that desired, excess pressure being dissipated by a portion of the gas bubbling through the column of liquid. Such a pressure regulator is very accurate when a relatively small rate of air flow is used. *E* is a calcium chloride drying tower.

The cell designed for holding the compacted powder is composed of a straight piece of glass tubing carrying ground in stopcocks at both ends. The cell is 25 cm long and has an internal diameter of 3.0 cm. One thickness of 20-mesh sieve cut to the proper size is cemented to the lower stopper to serve as a support for the mass of compacted particles during the measurement. In order to fill the tube the glass stopcocks are removed from the apparatus and a cork is placed in the lower end. This stopper contains a flat head screw of exactly the same length as the cork. It is placed in the cork so that its head is flush with the outer surface of the stopper. Cold, dry powder is then compacted against the cork stopper. When the compaction is complete the screw is removed from the cork which then can be taken from the glass tube without disturbing the mass of powder because of sudden changes in pressure. One or two disks of 20-mesh sieve are then inserted, followed by the ground in glass stopcock with its attached screen. The screen serves as a support for the compacted mass. Rubber bands hold the glass stopcocks in position. This arrangement gave checking results with different air pressures, indi-

[3] H. G. Botset, Rev. Sci. Inst. **2**, 84 (1931).
[4] Joseph Chalmers, D. B. Taliaferro and E. L. Rawlins, Trans. A. I. M. M. E. **98**, 375 (1932).
[5] M. Muskat and H. G. Botset, Physics **1**, 27 (1931).
[6] Coberly Stevens, Trans. A. I. M. M. E. **103**, 26 (1933).
[7] R. D. Wyckoff, H. G. Botset and N. Muskat, Physics **3**, 90 (1932).
[8] R. D. Wyckoff, H. G. Botset and M. Muskat, Trans. A. I. M. M. E. **103**, 219 (1933).
[9] E. C. Bingham, *Fluidity and Plasticity* (McGraw-Hill Book Company, New York, 1922), 1st Edition.

cating the elimination of error due to end effects.

After the loaded cell is in place, it is connected with the Venturi meter and manometers, and compressed air is admitted to the compacted mass by opening stopcock, *F*. The volume of air passing in unit time through Venturi, *G*, is measured by the flow meter, *C*. The manometers used in measuring the up- and downstream pressures on the compacted sample must be open to the air in order that the pressure drop in the sample may be calculated to an absolute basis (manometer reading+atmospheric pressure).

When very fine powders are compacted in the cell and air is passed through the mass a time lag always occurs before the downstream pressure builds up to a constant value. The length of time required for equilibrium to be attained depends on the size of the capillaries in the porous mass and on the volume of the system between the Venturi orifice and the cell. Consequently, the apparatus should be made as compact as possible and in every experiment care should be taken that equilibrium conditions are reached before readings are taken; usually 10 to 15 minutes are required to establish a constant pressure gradient for very fine powders.

A sudden reduction in the pressure applied to the compacted powder will cause cracks to appear in the sample. This happens because reduction in pressure within the sample cannot take place rapidly through the small capillaries without the formation of channels. The difficulty is avoided by making the measurements at progressively higher pressures; pressure being maintained on the sample throughout the course of the experiments or by shutting off the stopcock, *F*, ahead of the sample, thus allowing the pressure therein to be dissipated.

Preparation of Sample

Preparation of a satisfactory sample is the most important step in the determination of the average pore diameter in a compacted powder. Preliminary experiments were performed with briquettes prepared by the method described by Traxler, Baum and Pittman.[10] The briquettes were carefully sealed in a funnel or tube by means of paraffin and the volume rate of air passing through the powder measured for various air pressures, as described above. Although the briquettes were prepared very carefully and dried slowly in a desiccator over sulfuric acid followed by gentle heating in an electric oven, they usually contained cracks and fissures, the presence of which rendered permeability measurements valueless for estimating average pore diameter.

Compaction of the dry powder in the glass tube by hand or machine tapping was found to produce a sample which was uniformly packed and free from channels or fissures. However, uniform packing, which is absolutely necessary, occurs only when the sample is compacted to completion by the particular method used. When a loose packing is attempted by not compacting to completion a gradation in the degree of packing occurs throughout the sample. Thus, different states of packing must be obtained by different methods, such as hand or machine tapping, each being carried to the point where no further reduction in the volume of the packed powder is obtained.

Validity of Equations Used

In order to prove the general applicability of the equations used, measurements of average pore diameter were made on a silica dust by using various pressures and with samples of different length and cross-sectional area.

Two sets of data are given in Table I. These represent the extremes of applied pressure and sample size employed. Low pressures are used to avoid difficulties due to disruption of the sample, turbulent flow of the air through the capillaries and marked changes in the viscosity of the gas.

Table I. *Representative experimental data on silica dust.*

	Sample 1	Sample 2
Temperature	25°C	25°C
Percent voids, B	37.5	37.5
Sample length, l	10.0 cm	5.0 cm
Cross-sectional area of sample, A	6.06 cm²	3.90 cm²
Rate of flow, $\bar{q}$	0.0266 cm³/sec.	0.0224 cm³/sec.
P_1-P_2	62.3 g/cm²	39.7 g/cm²
Viscosity of air, η	1.85×10^{-4} poise	1.85×10^{-4} poise
Average pore radius, r	0.533μ	0.540μ

[10] R. N. Traxler, L. A. H. Baum and C. U. Pittman, An. Ed. Ind. Eng. Chem. **5**, 165 (1933).

The length and cross-sectional area of the sample as well as the applied pressure may be varied over a rather wide range without affecting the values obtained for average pore size.

Relation between Void Content and Pore Size

Measurements of the average pore diameter were made on compacted samples of pulverized black slate and silica. Values were obtained on each powder for three different states of packing, the compactions being obtained by hand and two different applications of a motor driven tapping machine, each sample being compacted to completion by the particular method employed. Table II shows the values obtained for the average pore diameter at various compactions (as indicated by different void contents).

Table II. *Percent voids—Pore diameter relationship.*

Powder	Percent Voids B	Average Pore Diameter d (microns)
Black slate	57.4	1.656
	62.1	1.964
	66.0	2.384
Silica	37.5	1.066
	44.7	1.448
	49.3	1.818

Fig. 2 shows these data with percent voids plotted on an arithmetic scale and average individual pore diameter on a logarithmic scale. For the range of packings studied the relationship between percent voids and average pore diameter in compacted powders may be expressed conveniently as

$$\log d = mB + b, \qquad (11)$$

where d = average individual pore diameter in cm,
B = percent voids,
m and b are constants.

Data were obtained on several other kinds of pulverized materials of widely varying characteristics and on particle size fractions of different powders. Particle size has no marked effect on the slope m of the percent voids *versus* logarithm of pore diameter curve, but governs the value of the intercept b. For all of the powders studied the average value for m was 0.019. For accurate work it is recommended that m be determined experimentally for every powder since particle shape and other specific characteristics may influence the value to some extent. Practically, 0.019 may be used for most commercially available powders.

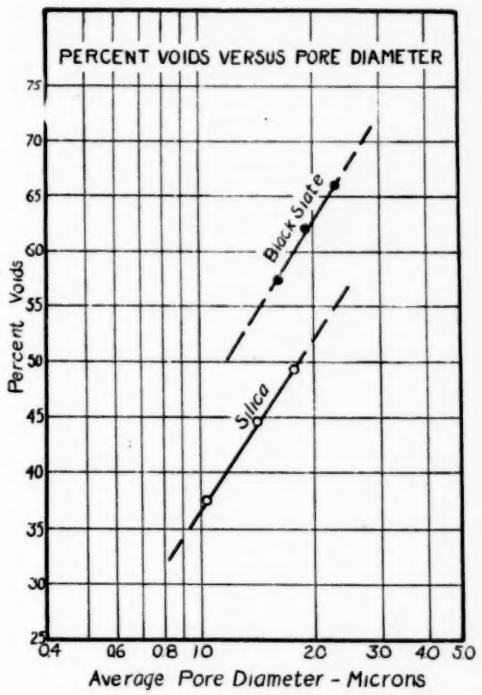

Fig. 2. Semilog plot of percent voids *versus* average pore diameter in compacted pulverulent material.

Assuming a value of 0.019 for m in Eq. (11) and with the pore diameter determined at any easily obtained void content the value of b for any mineral powder may be calculated. Then, with the constants m and b established for a particular powder the average pore diameter associated with any degree of compaction may be calculated.

Effect of Particle Size on Average Pore Diameter

Other factors being equal, an increase in the average particle size should cause an increase in average pore diameter. In order to establish the relationship between the average particle size and pore diameter, powders should be used which have particles of the same shape but different sizes. Various mineral powders had been fractionated in our laboratory using a Federal Air Classifier. Thus, permeability measurements

were made and the average pore diameters calculated for five size fractions of both slate and silica powder.

Table III gives the experimentally determined

TABLE III. *Particle size—pore diameter relationships.*

SIZE FRACTION (microns)	"b"	B_1 (%)	d_1 (microns)	B_2 (%)	d_2 (microns)	$D_{av.}$ (microns)
			Pulverized Black Slate			
2–5	−1.2712	70.3	1.16	55.0	0.594	3.50
5–10	−1.0299	66.6	1.72	55.0	1.036	7.50
10–20	−0.8089	63.7	2.52	55.0	1.722	15.0
20–40	−0.5716	60.9	3.85	55.0	2.974	30.0
40–80	−0.1961	54.8	7.00	55.0	7.060	60.0
			Pulverized Silica			
2–5	−0.9221	52.7	1.20	43.0	0.785	3.50
5–10	−0.5865	47.5	2.07	43.0	1.700	7.50
10–20	−0.3945	44.7	2.85	43.0	2.645	15.0
20–40	−0.0507	43.7	6.02	43.0	5.838	30.0
40–80	+0.1202	44.1	9.08	43.0	8.650	60.0

void contents and pore diameters B_1 and d_1, respectively, on the 2–5, 5–10, 10–20, 20–40 and 40–80 micron fractions of silica and slate dust. Using Eq. (11) and the assumed value of 0.019 for m, the pore diameters, d_2, were calculated at 55 percent voids for slate and 43 percent voids for silica. The average pore diameter could have been estimated for any other degree of packing.

In order to determine the influence of particle size on pore diameter it was necessary to maintain constant all the other factors (particle shape, size uniformity and degree of packing) which govern pore size. Microscopic examination shows that in general the particles in the different fractions of these powders all have about the same shape. Since the size limits of the fractions used had diameter ratios of 1 to 2, the particle size uniformity in all of the fractions was also constant. When the particle shape and size distribution in a powder is constant the degree of packing is measured by the percent voids; equivalent states of packing occur at equivalent void percentages. Therefore, the differences in pore size shown in column 6 of Table III for the various fractions of either slate or silica powder are due chiefly to particle size.

The last column in Table III gives the average diameter, D_{av}, of the particles present in each powder. It is evident that for a given state of packing a rather constant relationship exists between the average particle size of a compacted powder and the diameter of the average pore or capillary. For the degrees of packing given in column 5 of Table III the pore size of the compacted slate is one-seventh to one-tenth that of the average particle diameter; the pore diameter of the silica is about one-fifth as large as the average particle size. Nevin[11] found that the average pore diameter of compacted sand is one-fifth the diameter of the most frequent size particle.

ACKNOWLEDGMENT

The authors are indebted to Mr. C. U. Pittman for valuable suggestions during the development of the method, and to Mr. H. E. Schweyer for the drawings.

[11] Charles Merrick Nevin, Bull. Am. Assoc. Pet. Geol. **16**, 373 (1932).

The Copper Oxide Rectifier*

CHAUNCEY STARR,** *Rensselaer Polytechnic Institute*

(Received July 15, 1935)

The equilibrium diagram of the copper: copper oxide: oxygen system controls the conditions of formation of the cuprous oxide rectifier. The interface between the cuprous oxide and the copper from which it is formed can be studied with polarized light. Intimate contact exists for more than half the total area. The technique of preparing the rectifier has a marked influence on its characteristics. By using a method of measuring the resistance characteristic which did not cause an error due to current heating at the interface, unusual results were obtained from specimens made under various conditions. Measurement of the thermal conductance of the rectifier disclosed a new physical phenomenon, asymmetrical thermal conductance. This asymmetry is in the direction that would be expected from the electron theory of heat conduction.

INTRODUCTION

THE formation of cuprous oxide on copper at a high temperature produces a junction between the two that has an asymmetrical resistance. This asymmetry is utilized in the copper-cuprous oxide solid rectifier. The electrical resistance is lower in the direction of electron passage from the copper to the cuprous oxide than in the reverse direction. The junction between the cuprous oxide and the copper also has the property of developing an electromotive force when it is illuminated. This property is the basis of the copper-cuprous oxide solid photo-cell. The characteristics of the commercial cuprous oxide rectifier have been ably reported and discussed by Grondahl.[1]

THE SYSTEM COPPER: COPPER OXIDE: OXYGEN

The conditions that control the formation of the cuprous oxide rectifier and photo-cell can be determined from the equilibrium relations that exist between copper, cuprous oxide (Cu_2O), cupric oxide (CuO), and oxygen. These equilibrium relations are represented graphically by the pressure-temperature diagram of Fig. 1. The fixed points of the diagram, indicated in Fig. 1 by circles, and the data used for the calculation of the equilibrium triple curves were taken from the work of Roberts and Smyth,[2] Vogel and Pocher,[3] and Rhines and Mathewson.[4] The gas pressure plotted in Fig. 1 is the sum of the partial gas pressures of oxygen, cuprous oxide, and copper. The last two become appreciable only at very high temperatures or very low pressures. It is probable that at some very low pressure cuprous oxide sublimes. Feitknecht[5] has shown that the presence of N_2 or CO_2 has no effect on the equilibrium relations.

The temperature-concentration diagram of copper-cuprous oxide is given by Rhines and Mathewson.[4] The main point of interest in relation to the cuprous oxide rectifier is the eutectic mixture Cu—3.5 percent Cu_2O with a melting point at 1065°, corresponding to the vertical dotted line in Fig. 1. According to Vogel and Pocher,[3] below 375° cuprous oxide is not stable, and decomposes very slowly into a solid solution of oxygen in copper and into cupric oxide. The decomposition is extremely slow and cannot be found on the cooling curves. The existence of this decomposition has not been verified.

The partial pressure of oxygen in air is approximately 153 mm Hg. This is represented in Fig. 1 by the line *a–b*. The point *a* is the intersection of this gas pressure with the equilibrium curve of CuO, Cu_2O, and O_2, and corresponds to a temperature of 1026°. The point *b* corresponds to the eutectic temperature, 1065°.

* Part of a thesis presented by the author to the Rensselaer Polytechnic Institute for the degree of Doctor of Philosophy.

** Charles A. Coffin Fellow and Research Fellow in Physics, Harvard University.

[1] Grondahl, "Copper-Cuprous-Oxide Rectifier and Photoelectric Cell," Rev. Mod. Phys. **5**, 141 (1933).

[2] Roberts and Smyth, "The System Copper: Cupric Oxide: Oxygen," J. Am. Chem. Soc. **43**, 1061 (1921).

[3] Vogel and Pocher, "The System: Copper-Oxygen," Zeits. f. Metallkunde **21**, 333 (1929).

[4] Rhines and Mathewson, "Solubility of Oxygen in Solid Copper," A. I. M. M. E., Inst. Metals Div. Tech. Pub. 534 (1934).

[5] Feitknecht, "Oxidation of Copper at High Temperatures," Zeits. f. Elektrochemie **35**, 142 (1929).

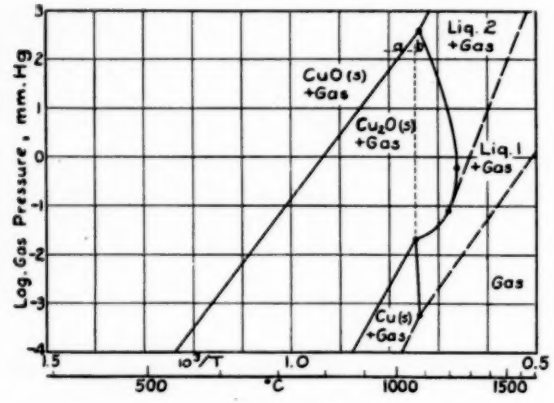

FIG. 1. Pressure-temperature equilibrium diagram of the system copper: copper oxide: oxygen.

During the formation of cuprous oxide, the pressure of the oxygen surrounding the copper being oxidized should lie in the Cu_2O equilibrium region of Fig. 1. The temperature should not rise above the eutectic melting point, 1065°. For oxidation in air at atmospheric pressure, the temperature should not fall below 1026°. The customary oxidizing temperature is 1040°. With reduced oxygen pressure, attained by means of pumps or mixture with inert gases, the minimum temperature for proper oxidation is lowered, in accordance with the CuO, Cu_2O, O_2 equilibrium curve. During the cooling of the specimen from the oxidation temperature the region of formation of CuO (black oxide) is entered. Even if the rate of cooling is slow (furnace cooling) only a thin film of black oxide is formed on the surface of the Cu_2O (red oxide). If the cooling is very rapid (water quench) it is possible to prevent the formation of the black oxide, but the rapid cooling causes the red oxide to crack off the copper due to unequal thermal contractions. It was found that the use of inert gases, N_2 or CO_2, with a small amount of O_2, permitted water quenching without cracking. Such specimens had a glossy red surface. If the oxidation of the copper is conducted below 1026° in air at atmospheric pressure, a layer of CuO is first formed which reduces the oxygen pressure at the copper underneath so that Cu_2O may be subsequently formed, provided the temperature is not too low. If the temperature is too low, a black film is formed which will not adhere to the copper. Apparently an intervening layer of red oxide is necessary to cause the adherence of the black oxide.

STRUCTURE OF THE COPPER OXIDE INTERFACE

The nature of the contact between the cuprous oxide crystals and the copper from which they grew has been a subject for speculation. It was found that by observing a specimen with a glossy red surface under polarized light, it was possible to focus under the surface of the oxide and observe structure. The technique pertinent to the instrument used for these observations and the interpretation of observed structure has been discussed by Dayton.[6] A specimen oxidized at 950° in tank N_2 (contains a small amount of O_2) for 20 minutes and then water quenched, was observed in this manner. Fig. 2A shows the appearance of the surface of the rectifier, and

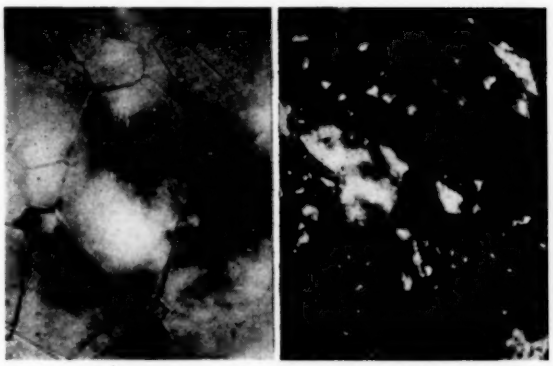

A B

FIG. 2. Cuprous oxide rectifier, ×500, crossed Nicols. A, surface of the rectifier, showing the ends of the cuprous oxide crystals; B, copper-cuprous oxide contact at the base of the crystals shown in A.

Fig. 2B shows the appearance of the contact directly underneath the crystals seen in Fig. 2A. Both photographs were taken at 500 magnification with crossed Nicols. The thickness of the cuprous oxide layer was 0.066 mm. The structure under the surface could not be observed with parallel Nicols. The bright regions in Fig. 2B are the places where the cuprous oxide crystals have broken away from the copper, probably due to

[6] Dayton, "Theory and Use of the Metallurgical Polarization Microscope," A. I. M. M. E., Inst. Metals Div. Tech. Pub. 593 (1935).

stress induced by the water quench. It is evident that intimate contact exists for more than half the total area. It does not seem, therefore, that the theories that assume point contacts between the copper and the cuprous oxide are tenable.

Determination of Rectifier Characteristics

The experimental work reported in this paper was performed on specimens one inch square prepared from electrolytic copper cut from 65 mil sheet. The applied metal contact was held against the surface of the rectifier with a pressure of 200 lbs./in.^{2} by means of a spring clamp. A constant temperature cabinet maintained the specimen at a temperature of 25°. The circuit used to measure the resistance-voltage characteristic was a resistance bridge. Since most of the rectifier resistance, in the high resistance direction, is concentrated in a thin layer at the natural interface between the base copper and the cuprous oxide formed from it, a small current flow in this direction raises the temperature of the interface markedly. This temperature rise appreciably lowers the resistance of the rectifier, so that the measurement of the resistance under a condition of continuous current flow gives too low a value (sometimes half the cold resistance) and the actual temperature of the interface is not known. In order to prevent this effect, a cam was used to periodically send a current through the bridge circuit. The period of the cam was 15 seconds, and the circuit was closed for about 1 second. This gave sufficient impulse to the galvanometer to allow the bridge to be balanced, but did not heat the rectifier appreciably and also allowed a long time for it to cool. After the bridge had been balanced, an equivalent resistance was substituted for the rectifier, the current circuit was closed, and the voltage across the equivalent resistance was measured with a potentiometer.

Typical results of the measurements are shown in Fig. 3 and Fig. 4. The figure captions give the preparation sequence of the specimens. Fig. 3, curve 1, shows the typical characteristic curve of a low resistance rectifier. The resistance has a maximum at about 1.6 volts. Grondahl[1] states that all the rectifiers have a similar maximum between 0.75 and 1.5 volts. That this is not so

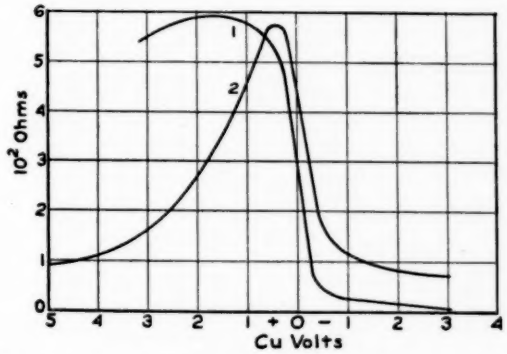

Fig. 3. Resistance-voltage characteristics. Curve 1, specimen oxidized in air at 1040°, furnace cooled, annealed in air at 500° for 3 hours, and water quenched. Aquadag on Cu_2O surface. Curve 2, specimen oxidized in tank N_2 at 950° for 20 minutes, water quenched, annealed in vacuum at 600° for 12 hours, and vacuum quenched. Aquadag on Cu_2O surface.

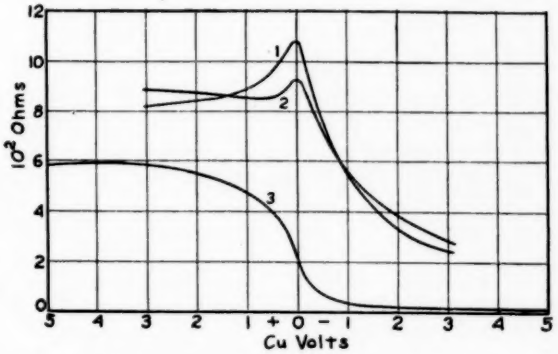

Fig. 4. Resistance-voltage characteristics of specimen oxidized in tank N_2 at 1000° for 10 minutes, and water quenched. Curve 1, CuO surface untouched. Curve 2, Cu_2O surface. CuO removed by NaCN etch. Curve 3, Aquadag on Cu_2O surface.

can be seen from the other curves. Fig. 4, curve 3, has a maximum at about 4 volts, curve 2 has a minimum at about 0.7 volt. Many specimens had no maximum below 5 volts. It is evident from a study of the curves that the treatment of the applied contact surface has a large effect on the shape of the rectification characteristic. This surface contact resistance does not behave like a series resistance. In many cases, a treatment of this surface contact that causes a resistance decrease in the low resistance direction causes a very much greater decrease of resistance in the high resistance direction. Fig. 3, curve 2, is of interest since it represents an attempt to remove from the Cu_2O of the rectifier as much CuO and O_2 as possible. The resistance char-

acteristic is very unusual as very little asymmetry is present. Fig. 4, curve 1, shows a characteristic that was found to be quite general. All resistance curves for specimens that had CuO on the surface showed a maximum at or near zero voltage, and decreased exponentially on both sides of this maximum.

It has been definitely ascertained by Grondahl[1] and others that the resistance asymmetry occurs at the Cu_2O–Cu interface, and that the Cu_2O layer forms only a very small portion of the total resistance. It is evident from the experimental work here presented that the phenomenon is complicated by the behavior of the Cu_2O layer and the surface contact. A combination of the wave-mechanical action of a potential barrier at the interface and the action of a space charge in the Cu_2O might possibly explain the experimental results.

Thermal Conductance of the Cuprous Oxide Rectifier

No measurement of the thermal conductance of the cuprous oxide rectifier is reported in the literature. Vogt[7] measured the thermal conductivity of cuprous oxide. Using the comparison method, and quartz as the comparison substance, he found the thermal conductivity of cuprous oxide at −78° to be 0.019, at 0° to be 0.015, at 100° to be 0.017 cal./sec. cm² (°C/cm).

The apparatus used in this investigation to measure the thermal conductance of the cuprous oxide rectifier was similar to Vogt's. The only material available that had approximately the same thermal conductance as the rectifier was thin paper, of the type used to roll cigarets. This was used as a comparison standard. The arrangement of the apparatus is indicated in Fig. 5. The heat was supplied through a nichrome heating coil wound about the top brass block. The brass block at the cold end was cooled by a coil of copper tubing, embedded in Wood's metal, through which tap water ran. All faces had a cross section area of 1 in.², and were polished smooth with 3/0 emery paper. The rectifier used was the specimen whose resistance-voltage characteristic is shown in Fig. 3, curve 1.

[7] Vogt, "Electrical Determinations with Cu_2O," Ann. d. Physik **7**, 183 (1930).

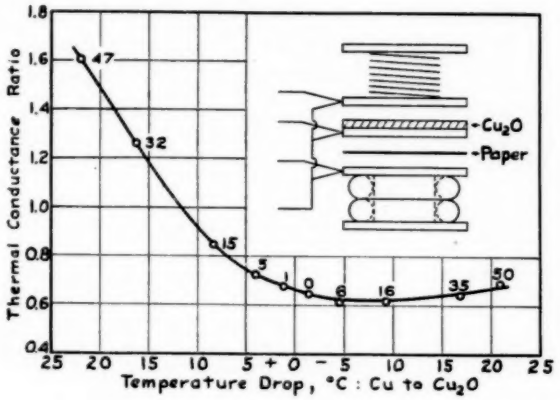

FIG. 5. Thermal conductance ratio, rectifier: paper, *vs.* temperature drop across the rectifier. The temperature above room temperature of the Cu_2O–Cu interface during the measurement of the ratio, is given beside each point.

Thermocouples of nichrome-advance wire were embedded in small holes in the sides of the brass blocks and in the copper of the rectifier, as indicated in Fig. 5. The advance wires of the thermocouples were connected together and the four leads brought to a cold junction held at room temperature. The whole assembly was held in a large *C* clamp, insulated from the jaws by asbestos board, and surrounded by a cylinder of asbestos paper to prevent air currents. The temperature gradient across the cuprous oxide was adjusted by varying the current through the heating coil. With the apparatus as arranged in the figure, the heat flowed from the Cu_2O to the copper, and with the rectifier reversed, so that the paper was above the copper and the Cu_2O was below, the heat flowed from the copper to the Cu_2O. The time required for the thermal equilibrium to be established was about 15 minutes. The thermocouple voltages were read with a Wolff potentiometer by using a galvanometer sensitive enough to allow the determination of microvolts.

When equilibrium was established, the ratio of the thermal conductances of the rectifier and the paper was equal to the inverse ratio of their temperature drops, assuming that the heat loss from the sides and through the center thermocouple was negligible. This assumption was tested after the measurements on the rectifier had been made by removing the cuprous oxide from the copper slab and placing paper in the

top and bottom positions. Measurements of the ratio of the thermal conductances of the two papers were then made for different temperatures of the hot end. It was found that the ratio decreased by about 1 percent when the temperature of the hot end was raised from room temperature to 80° above room temperature. This error is of the order of the precision of the measurement, and so was disregarded. This measurement also indicated that the thermal conductivity of the paper did not change appreciably with temperature.

The results of the measurements are plotted in Fig. 5. Beside each point on the curve is given the temperature of the Cu_2O-Cu interface above room temperature.

The thickness of the cigaret paper was 0.026 mm. The *International Critical Tables* give as the thermal conductivity of paper 0.00011 cal./sec. cm² (°C/cm). The thermal conductance of the paper was thus 0.042 cal./sec. cm² °C. The thickness of the cuprous oxide layer of the rectifier, found from the thickness of the rectifier before and after removal of the oxide, was 0.0629 mm. With Vogt's[7] value for the thermal conductivity of the oxide, the thermal conductance of the oxide layer was 2.46 cal./sec. cm² °C at 24°. The measured ratio between the thermal conductances of the rectifier and the paper was about 0.66 at zero temperature gradient, or the total thermal conductance of the rectifier was approximately 0.028 cal./sec. cm² °C. The thermal conductance of the interface was thus 0.0283 cal./sec. cm² °C. Since the thermal conductance of the cuprous oxide layer is so much greater than that of the interface, the change of the thermal conductivity of the cuprous oxide with temperature can be seen to have a negligible effect.

The results indicate that there exists an asymmetrical thermal conductance characteristic in the cuprous oxide rectifier. The thermal conductance is larger in the direction in which the electrical conductance is larger, i.e., from the copper to the cuprous oxide. This would be expected from the electron theory of heat conduction. The asymmetry is apparently a property of the interface. The temperature characteristic of the interface is unknown, but while it probably affects the values of the thermal conductance it can not explain the observed asymmetry. As can be seen from the figure, for equal and opposite temperature gradients across the rectifier, the temperature of the interface was about the same, although the thermal conductances were different.

A more exact study of this phenomenon is necessary. The apparatus should be so arranged that the temperature of the interface remains constant throughout the measurement. A comparison material more reproducible than paper, and about which more is known, should be used.

The Electrical Conductivity of Glass

Part III. Current-Voltage Relationships with Highly Resistant Layers

H. R. KIEHL, *Pennsylvania State College*

(Received September 25, 1935)

Some effects upon current-voltage and temperature relationships as caused by the formation of "impregnated" layers in the vicinity of the electrodes are described. For "unimpregnated" samples, Ohm's law appeared to be valid. Upon "impregnation" various current-voltage relationships from $I=AV^N$ to that of Poole were observed, the nature of the function apparently depending upon the characteristics of the layers produced. The Rasch and Hinrichson equation was found valid for fresh samples over the range of temperatures used, but the presence of these layers caused distinct changes in the characteristics of this relationship. The possible importance of such layers upon the electrical properties of glass and other insulating materials at the higher fields and temperatures and their possible effect in causing some of the apparent discrepancies in existing data is pointed out. The importance of much further detailed study of their properties is suggested.

I. INTRODUCTION

CONSIDERABLE variation seems to exist between current-voltage relationships reported for electrical insulating materials, including glass, especially at higher field intensities. In glass, for low field intensities, Ohm's law has been found valid over a considerable range in temperature by various investigators. For higher fields, a number of variations seem to occur. Mundel[1] found the relation between the current and the field intensity in glass to be of the form $I=CE^K$, where $K=2$. Poole[2] found a logarithmic relationship of the form $I=aXe^{bX}$, where I is the final constant conduction current and X is the field intensity; this relation seemed valid for fields as high as 10^6 volts/cm. Schiller[3] verified this law for glass and mica for fields of the same magnitude. Hubmann[4] later also found this relationship for specimens of glass 1 to 4 microns thick, with the same field intensities. However, few results for such high fields at higher temperatures than the relatively low ones used by these observers seem available. Somewhat similar results to those mentioned for glass have also been obtained on various other materials. Hochberg and V. Joffe[5] found a relationship for saltpeter crystals somewhat analogous to that of Mundel on glass which could be expressed in the form $\sigma_r=kV^\alpha$, where σ_r was the final conductivity; V the applied voltage and α and k, constants. The value of α was found to be greater than or equal to zero, approaching zero as the temperature was increased. Such apparent deviations from Ohm's law have been explained by some as due to variations in the value of an existing polarization potential, P, showing that in many cases P increases more slowly than in direct proportion to V. Such variations of P seem to have been observed for a number of materials. There are still, however, other instances of nonlinear current-voltage relationships, in which no appreciable polarization e.m.f.'s were reported.

The possible importance of highly resistant anode layers in producing such variations in current-voltage relationships in glass was suggested by the results of Le Blanc and Kershbaum,[6] Guntherschülze,[7] and Ferguson, Mulligan and Rebbeck.[8] Le Blanc and Kershbaum found the relation $I=KV^2$ to be valid in glass at high temperature with the presence of such anode layers. Ferguson, Mulligan and Rebbeck found Ohm's law verified for fresh samples, but with penetration of the layer found a gradual change to the relationship $\log I=A-BE$ for lower voltages. For higher voltages this relation-

[1] E. Mundel, Archiv f. Elektrotechnik **15**, 320 (1925).
[2] H. H. Poole, Phil. Mag. **32**, 112 (1916); **34**, 195 (1917); **42**, 488 (1921); Nature **107**, 534 (1921).
[3] H. Schiller, Ann. d. Physik **83**, 137 (1927); **81**, 32 (1926); Archiv f. Elektrotechnik **17**, 609 (1927).
[4] H. Hubmann, Ann. d. Physik **9**, 733 (1931).
[5] B. Hochberg and V. Joffe, Zeits. f. Physik **66**, 172 (1930).
[6] M. Le Blanc and F. Kershbaum, Zeits. f. physik. Chemie **72**, 468 (1910).
[7] A. Guntherschülze, Ann. d. Physik **37**, 435 (1912).
[8] J. B. Ferguson, M. J. Mulligan and J. W. Rebbeck, J. Phys. Chem. **32**, 1018 (1928).

ship again apparently changed to the original linear one between I and V. This behavior could be explained by a variation in the polarization e.m.f. which occurred with the production of the layers, and which fell off to small values for higher fields. The law, $(V-P)/R=I$, as expressed by Joffe and others, seemed valid in this case.

Because of the apparent ease of formation of such layers at higher fields and temperatures, and their probable effect upon the electrical properties of glass, it was considered of value to continue investigations of these effects. A somewhat greater range in fields and different conditions of layer formation than those employed by Ferguson, Mulligan and Rebbeck, were used. It was felt that such continued studies of the effects of these layers might furnish an explanation of some of the apparent anomalies which have been observed in the electrical behavior of insulating materials. The results of one preliminary group of such investigations are given here. The data presented represent only a very small portion of that necessary for complete information, but serves to emphasize the importance of further studies of this phenomenon.

II. Apparatus

The apparatus, circuit, and type of glass samples used for these tests have been described in previous papers.[9] Representative data are here given on two samples, (1) of average thickness 0.212 mm, and (2) 0.170 mm. The maximum fields used were 3.7×10^4 volts/cm.

III. Procedure

The procedure used has been described previously.[9, 10] A brief repetition will be given here. While the temperature of the sample was kept constant, the final equilibrium current was measured for each of a definite group of increasing fields. In each case where a reversible absorption current was noted, the value of the current used was the final constant value. At higher temperatures, where no such reversible absorption currents could be observed, the constant value of the current was taken as soon as possible after the application of the field to avoid formation of the anode layers described previously.[9, 10] At still higher temperatures, however, it became impossible to obtain reliable values of the steady current, because of the rapidity at which such layers were formed. The highest temperatures which could be used with present apparatus were therefore limited by this condition. The penetration of the electrode ions was then allowed to occur for a given period of time. The sample was allowed to cool to room temperature and series of observations similar to those made on the fresh sample were made. In every case the sample was discharged through the measuring circuit between each application of the field. Each run, then, consisted of observations of the final constant value of the conduction current for a given number of voltages, the temperature remaining constant. Succeeding similar runs were made at increasing temperatures. Between all constant temperature group runs, the sample was short-circuited, and allowed to return to room temperature for various periods of time, from several hours to several days. In one case a sample was allowed to remain short-circuited for two months, before a new series of tests was made, to determine, to some extent, the permanency of these effects. Several successive "impregnations" were made on each sample with a series of runs as outlined occurring after each "impregnation."

IV. Results

Results somewhat similar to those of Ferguson, Mulligan and Rebbeck were obtained. For an "unimpregnated" sample, a linear relationship was observed between current and applied voltage, for temperatures between 22°C and 213°C (Fig. 1, curve A).

After the first impregnation, a deviation from this linear relationship occurred (Fig. 1, curve B). Successive impregnations caused an increase in this deviation (Fig 1, curve C). In some cases, a slight tendency towards a linear relation was noticed at the higher fields for the smaller impregnations; in others this effect was not observed. Higher fields than those available appear to be necessary to show such linearity,

[9] H. R. Kiehl, Physics **5**, 363 (1934).
[10] H. R. Kiehl, Physics **5**, 370 (1934).

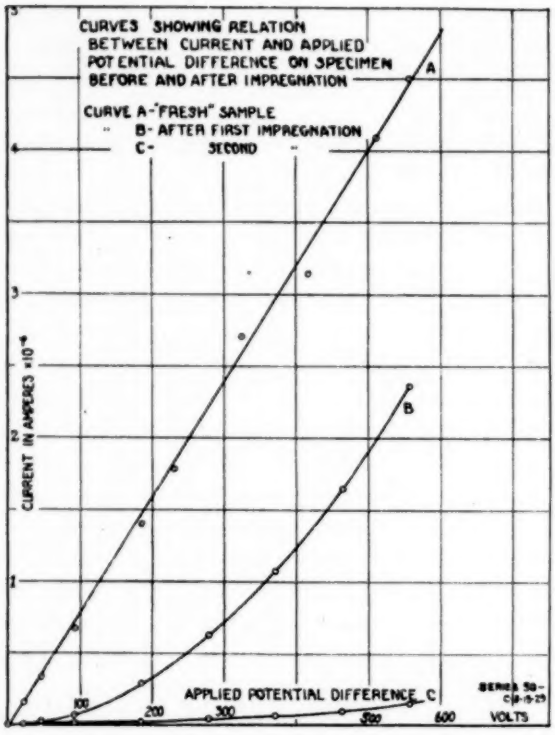

FIG. 1. Curves showing relation between current and and applied potential difference on specimen before and after impregnation. Curve *A*, "fresh" sample; curve *B*, after first impregnation; curve *C*, after second impregnation.

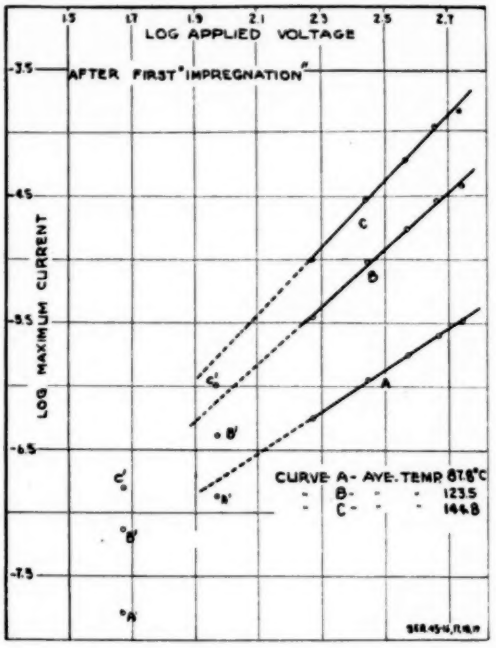

FIG. 2. Maximum current *vs.* applied voltage:

Values of constants in $I = AV^N$ for curves A, B and C

CURVE	AV. TEMP.	N	A
A	87.8°C	1.63	1.11×10^{-10}
B	124	2.22	3.37×10^{-11}
C	145	2.59	1.39×10^{-11}

if it exists in all cases. Curve *C* shows the relationship between current and voltage for one sample two months after a second impregnation, the sample being short-circuited at room temperature during this time interval. Tests made a short time after impregnation showed similar results.

At temperatures up to about 50°C, a polarization e.m.f. could be observed with the apparatus available; at higher temperatures no values sufficient to explain the curvature in the current-voltage relationships could be measured. This may have been due to the slowness of the measuring instruments used, for in few cases could reliable measurements of the currents or the polarization e.m.f.'s be made less than 15 seconds after the field was applied or removed. Any e.m.f.'s which may have existed must have decreased to very small values within this time period.

Current-voltage relationships were investigated after various degrees of impregnation. As previously described,[10] current increases with time of field application were usually observed after the first such impregnation. In these cases, values of the maximum equilibrium current were used to determine this relationship. A typical case, that of the sample referred to above[10] (Sample No. 1), after an impregnation involving a charge of 2.7×10^{-2} coulomb, this maximum current, I, appeared to be related to the applied voltage, V, in the manner expressed by the equation

$$I = A V^N$$

(Fig. 2, curves *A*, *B*, *C*). Values of N appeared to increase from approximately unity at 23°C to 2.6 at 145°C. Values of A showed a decrease with temperature. Values of these constants are shown in the caption of Fig. 2. Deviations from this relationship, such as those shown by the points *A'*, *B'*, *C'* of Fig. 2, occurred in some cases.

For the next temperature used, 179°C, a change to the form

$$\log I = \log A_1 + BV$$

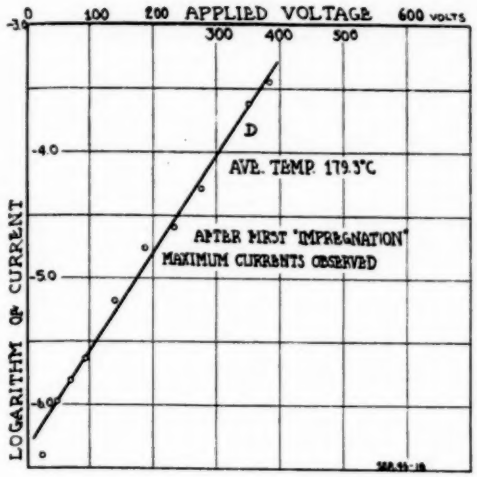

FIG. 3. Maximum current *vs.* applied voltage after first impregnation.

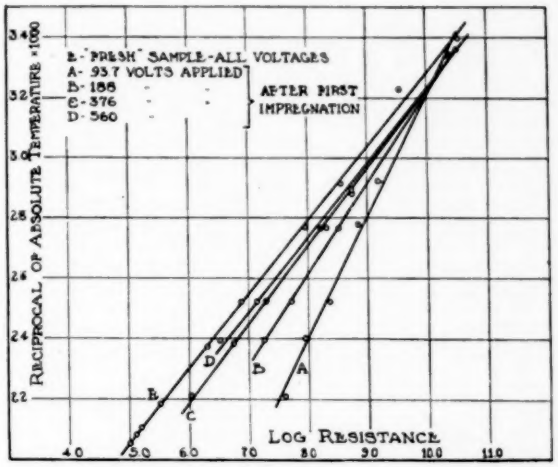

FIG. 4. Reciprocal of resistance *vs.* temperature for various voltages:

Values of the constants in $\log R = A' + B'/T$

CURVE	VOLTAGE	A'	B'
A	93.7 volts	+2.04	2480
B	188	−0.568	3280
C	376	−2.41	3850
D	560	−2.84	3970
E	Average for all voltages	−3.41	4090

seemed to occur (curve *D*, Fig. 3). This may have been due to changes occurring because of further impregnation, since higher temperatures showed further noticeable effects of such phenomena.

The electrical resistance, R, obtained from values of applied voltage and corresponding saturation currents, appeared to be related to the sample temperature in the manner specified by the Rasch and Hinrichson relationship,[11] *viz.*,

$$\log R = A' + B'/T.$$

This relationship appeared valid for the sample both in the original unimpregnated state and after the first impregnation referred to above (Fig. 4). For the sample in the original state, A' and B' were practically constant for all voltages used (curve *E*, Fig. 4). After the impregnation described, values of B' increased with increase in V, approaching those for the unimpregnated sample (curves *A*, *B*, *C*, *D*, Fig. 4). Values of these constants for the curves are shown in the caption of Fig. 4.

Whether values of A' and B' for the impregnated sample approach those for the glass in its original state as a limit, cannot be definitely stated because of limitations in available fields.

A second impregnation of the sample was then made at a temperature of 215°C, with 560 volts applied to the sample for 150 minutes.[12] Subsequent tests showed a rather good agreement with the Poole relationship in the form

$$\log R = \alpha - \beta V$$

where R is the final constant value of the resistance and V is the applied voltage. This relationship appeared valid over the entire voltage range used, 45 to 560 volts, and at least from 70°C to 140°C. Individual deviations and irregularities appeared to increase with further increase in temperature. Below 70°C, relationships were difficult to obtain with any degree of certainty because of rather small galvanometer deflections.

Several typical relationships are shown in Fig. 5. The values of β', the coefficient when the field intensity in volts per cm is used, appear to be approximately one hundred times those obtained by Schiller, Poole and Hubmann if the field is measured in corresponding units. The significance of this fact, considering the type of glass and the temperatures here used, is not entirely clear. It does suggest, however, a stress gradient through this impregnated layer much

[11] E. Rasch and F. W. Hinrichson, Zeits. f. Elektrochemie **14** (1908).

[12] H. R. Kiehl, Physics **5**, 363 (1934). See Fig. 6.

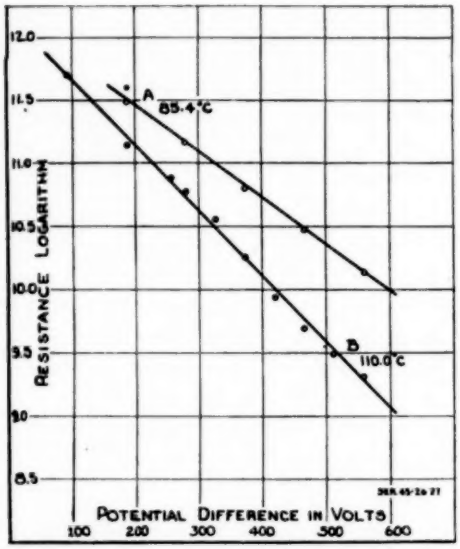

FIG. 5. Log of resistance *vs.* applied voltage. Curve *A*, temperature 85.4°C; curve *B*, temperature 110°C. Values of α and β in $\log R = \alpha - \beta V$ for several temperatures. The last column, β' shows the value of the coefficient when the field intensity in volts per centimeter is used.

TEMPERATURE	α	β	β'
85.4°C	12.2	3.64×10^{-3}	7.72×10^{-5}
110	12.2	5.22×10^{-3}	1.11×10^{-4}
140	11.6	5.86×10^{-3}	1.24×10^{-4}

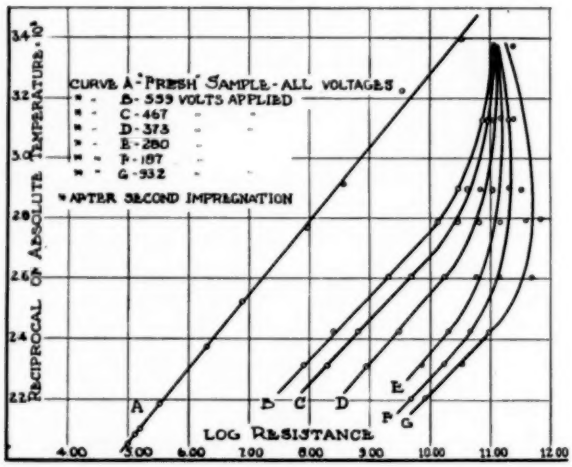

FIG. 6. Final resistance R *vs.* reciprocal of temperature.

in excess of that throughout the remainder of the sample, with a possible thickness of this layer of about 2 microns.

The relationships between the final resistance, R, and the temperature, T, obtained after this second impregnation of the sample are shown in Fig. 6 for a number of applied voltages (curves B to G). Curve A again represents this relationship for the unimpregnated sample. A less rapid decrease in R was observed over the lower temperature range, the relationship gradually changing, at higher temperatures, to a form apparently similar to that for the unimpregnated sample. Curves showing the relationship between $\log R$ and $1/T$ again approached that for the unimpregnated sample as the applied voltage was increased, with an apparent decrease in curvature at lower temperatures. Values of A' and B' over the rather limited linear portions of the curves appeared to vary from -1.2 to -3.0 and from 4700 to 5000, respectively. Relationships at higher fields could not be determined because of limitations in applied voltage.

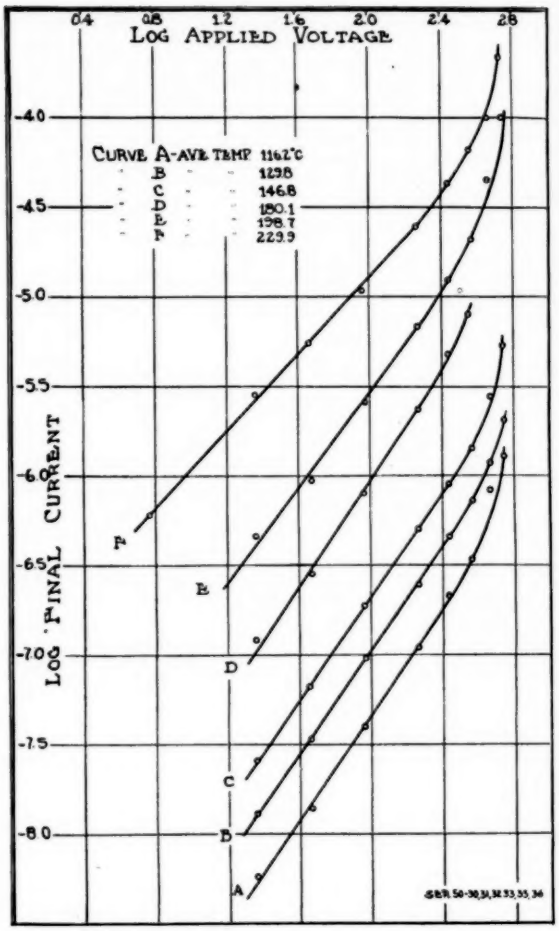

FIG. 7. Final current *vs.* applied voltage.

Further investigations on other similar samples produced, in general, analogous results. The nature of the relationships between current,

voltage and temperature appeared, however, to be definitely a function of the conditions of sample impregnation and of the nature of this impregnated layer. Slight variations here seemed to cause corresponding variations in the relationships observed.

The possible permanency of the effects produced by impregnated layers is shown by the results obtained on a second sample (No. 2) in which a series of tests was made several months after the impregnation was completed. The sample was short circuited at room temperature during the intervening period. Current-voltage relationships at this time appeared to follow the form $I = A V^N$ for fields as high as 10^4 volts/cm with the value of N varying from unity at 22°C to a rather constant value of 1.4 at higher temperatures. Values of A here seemed to increase with increase in temperature. At fields above 10^4 volts/cm noticeable deviations from this relationship occurred which appeared to increase with increase in temperature. Results for a number of temperatures are shown graphically in Fig. 7.

Present investigations are insufficient in scope to allow a completely systematic study of the phenomena described, but definitely indicate the probable importance of such impregnated layers in the electrical behavior of glass and other insulating materials. A further investigation of the characteristics of these layers seems of distinct value. The effects upon current-voltage and current-temperature relationships point to their possible importance in various apparent discrepancies observed by previous investigators and suggest a possible partial explanation of some of the present anomalies in the electrical characteristics of glass and other materials. The importance of such layers might be expected to be a function of the characteristics of the insulating and electrode materials, as well as of the temperature and applied field, rising with increase in this temperature and field.

The author again wishes to express his sincere appreciation to Dr. W. R. Ham, Dr. W. P. Davey and Dr. D. C. Duncan for valuable suggestions and kind interest in the work, and to Dr. J. T. Littleton and Dr. E. M. Guyer of the Corning Glass Works for helpful criticism in the preparation of the manuscript. Most sincere thanks are also extended to the Society of Sigma Xi for financial aid in the work at a time when continuation without this aid would have been extremely difficult.

Surface Tension of Molten Glass

W. B. PIETENPOL, *Department of Physics, University of Colorado*

(Received September 15, 1935)

The surface tensions of a number of different glasses have been determined by a new method. The method is termed "The Bulb Method" and is similar to the soap bubble experiment in which the excess of pressure within the bubble can be balanced against a small head of liquid in a manometer. The weight of the glass bulb is taken into consideration. The method is applicable to a temperature range of approximately 200°C above the annealing point of the glass. The variation of surface tension with change in temperature over the upper range of temperature investigated is found to be of the order of 0.04 dyne per cm per degree C. The magnitude of the surface tension for this range varies from 230 to 360 dynes per cm depending upon the kind of glass. A survey of previous results on surface tension discloses values of widely different magnitudes. One group of experimenters has obtained values of the order of 150 dynes per cm and another group, values of approximately 400 dynes per cm. The results obtained by the bulb method fall approximately midway between the values obtained by previous experimenters.

INTRODUCTION

WIDE discrepancies in the published values of the surface tension of molten glass have led the author to attempt measurements by an entirely new method.

The results of previous experimenters seem to be divided into two divisions, one group obtaining values of the order of 150 dynes per cm and the other group, values of approximately 400 dynes per cm. There seems to be no satisfactory explanation of the wide variation in results. A preliminary report[1] of the present investigation indicated results for different glasses of the order of 250 to 350 dynes per cm. Recent unpublished work by C. W. Parmelee and K. C. Lyon at the University of Illinois, using the maximum bubble-pressure method, gives values in good agreement, and it therefore seems advisable to present a more detailed description of what has been called "The Bulb Method."

HISTORICAL

Probably the first determinations of surface tension at high temperatures were made by Quincke about 1868. His method, known as the drop-shape method, consisted in observing the shape of the drop of the material when placed on a flat plate. Determinations of the surface tensions at high temperatures were made by Jaeger[2] on a large variety of substances by what is called the bulb pressure method. It consists in finding the pressure necessary to force bubbles of air or other gases through a capillary tube whose end dips beneath the surface of the liquid. A feature of Jaeger's article is the outline of surface tensions determinations made by others but unfortunately Jaeger made no determination on glass.

The drop weight method has been used by a number of observers, perhaps first of all by Tillotson.[3] The method is based on Tate's law which states that the weight of a drop falling from a tip is proportional to the diameter of the tip. In Tillotson's work it seems questionable whether one is justified in assuming that the diameter of the supporting surface film is the same as the diameter of the rod. He obtained values of surface tension for glass of the order of 100 to 150 dynes per cm, but in his summary states "that these values obtained for surface tension are probably not the absolute values, for, as Lord Rayleigh showed in the case of water, this method gives values only slightly greater than one-half the true values." There seems to be some uncertainty as to the accuracy of the method as Lecrenier,[4] working with glasses at temperatures of 1000° to 1200°, obtained values of 400 or more dynes per cm.

[1] W. B. Pietenpol and H. H. Scott, Phys. Rev. **35**, 296 (1930).

[2] F. M. Jaeger, "Über die temperaturabhangigkeit der molekularen freien oberflaschenergie von flussigkeiten." Zeits. f. anorg. allgem. Chemie **101**, 1 (1917).

[3] E. W. Tillotson, Jr., "Surface Tension of Molten Glasses," J. Ind. Eng. Chem. **3**, 631 (1911); also **4**, 651 (1912).

[4] Ad. Lecrenier, "Mesure de la Tension Superficielle du Verre," Bull. Soc. Chim. Belg. **33**, 119 (1924); **34**, 27 (1925).

In connection with his work on the strength of materials, Griffith[5] has determined the surface tension of glass at various temperatures. He obtained a value of 403 dynes per cm at 1100°C by the drop method, but probably the drop-shape method is meant as he speaks of it as Quincke's method. Other values of the same order of magnitude were obtained by observing the sag of glass fibers when supporting known weights, but not enough details of the work are given to form an adequate idea of its value and there is a question as to the correctness of the formula given.

Washburn and Libman[6] performed an extensive set of determinations by what they term the dipping-cylinder method and their values are most generally accepted at the present time. In the opinion of the writer the assumption that the angle of contact has a zero value is without sufficient experimental justification and for this reason their values may be too low. They obtained results over the temperature range of approximately 1200 to 1450°C, the values of surface tension ranging from 150 to 167 dynes per cm at 1206 and from 128 to 158 dynes per cm at 1454°C. They found for one glass that the rate of change of surface tension with temperature was very small at 1206°C and increased to about 0.08 dyne per cm per degree at 1454°C. The fact that Washburn and Libman's values are in general agreement with those of Tillotson is of no particular significance, because of the uncertainty of the absolute values of Tillotson's results.

The Bulb Method

The new method of determining the surface tension of glass devised by the writer is termed "the bulb method." It is similar to the familiar soap-bubble experiment, in which the excess of pressure within the bubble can be balanced against a small head of liquid in a manometer. The relationship between the excess pressure above atmospheric pressure and the other quantities involved, namely the diameter of the bubble, B, and the surface tension γ, is as follows:

$$2\pi B\gamma = \pi B^2 p/4,$$

from which the surface tension,

$$\gamma = pB/8.$$

In this work a thin glass bulb, blown on the end of a tube, was substituted for the soap bubble. The tube was attached to a manometer and bulb and tube were heated in an electric furnace to a temperature above that of the softening point of the glass. In the application of this method to glass, it was found that certain corrections which will be mentioned later needed to be introduced.

Apparatus

In the preliminary experiments a difficulty was encountered in supporting the glass. When a bare tube supporting a bulb was placed in the furnace and heated to the softening temperature, the tube would collapse if supported from below or draw out if hung from above. This difficulty was overcome, as shown in Fig. 1, by enclosing the glass tube in a suitable metal tube cooled by means of a water jacket at the outside end. The metal used was copper on account of its high thermal conductivity. This arrangement prevented any softening of the tube but there was still the necessity of adequately supporting the bulb. To accomplish this a collar of plaster of Paris somewhat smaller in diameter than the bulb was moulded about the base of the bulb for each determination. It was found desirable to allow the plaster collar to dry out slowly and thoroughly as otherwise there was danger of cracking when heated.

The end of the glass tube was connected to a water manometer, the readings of which were made with a vernier telescope. The door of the electric furnace was closed by means of asbestos board through which openings were made for the tube support and for observation. The furnace was mounted with its opening underneath to maintain as uniform a temperature as possible and lessen convection currents when an opening was made to observe the bulb diameter. This diameter was measured by means of a cathetometer mounted in a position such that the telescope

[5] A. A. Griffith, "The Phenomena of Rupture and Flow in Solids," Phil. Trans. Roy. Soc. **A221**, 163 (1920).

[6] E. W. Washburn and E. E. Libman, "Surface Tensions of Glasses at High Temperatures," Univ. of Illinois Engineering Experiment Station, Bull. No. 140 (1924).

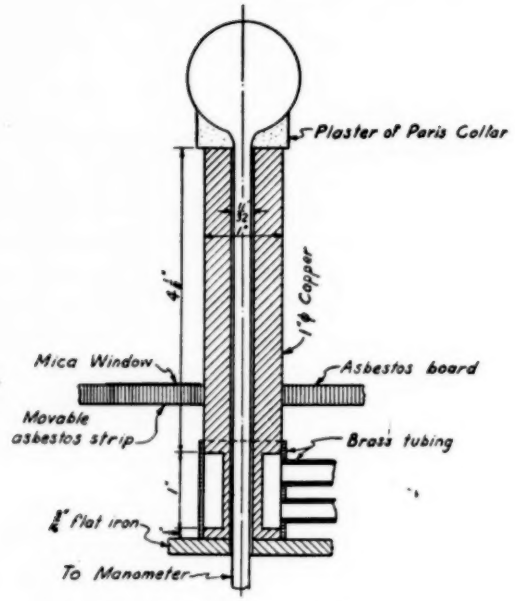

FIG. 1. Method of supporting bulb in furnace.

moved along a horizontal scale. In the final trials the opening was kept covered by a sheet of mica, in order to prevent a chilling of the bulb when measurements were taken. The temperature measurements were made by means of a platinum *vs.* platinum-rhodium thermocouple.

It was found to be important to use a thin bulb and one at the same time uniform and symmetrical. Preliminary trials with bulbs which were not uniform and symmetrical showed a tendency to collapse at a comparatively low temperature. Suitable bulbs for the purpose were blown by a skilled glass-blower. In size the bulbs ranged from 3.5 to 5.0 cm in diameter.

EFFECT OF WEIGHT OF BULB

In the formula given for the case of a soap bubble the weight of the soap film is assumed negligible. This is not permissible however in case of a glass bulb of higher density and greater thickness. In the preliminary tests using this simple relationship, it was found that the value of the surface tension in different tests did not agree well for samples of the same glass. There was also a considerable difference in the values found for the surface tension when the bulb was supported from below and when it was hung from above, the value always being lower when the bulb was in the latter position. This difference was attributed to the fact that the weight of the glass film needed to be considered.

If the bulb is supported from below the upward force is due entirely to the internal pressure in the upward direction. The downward force is the sum of the forces due to surface tension and the weight of the upper half of the bulb. Since these forces balance,

$$2\pi B\gamma + W = \pi B^2 p/4,$$

where W is the weight of the upper half of the bulb; and the surface tension

$$\gamma = pB/8 - W/2\pi B.$$

If the bulb is hung from above,

$$\gamma = pB/8 + W/2\pi B.$$

Thus if determinations were made in both positions, on bulbs of equal dimensions and weights, the true value of the surface tension would be the average of the two values found. In the preliminary trials the weights of the bulbs were not determined but the difference between the results were of the order of magnitude which the above equations would lead one to expect.

In the final experiments and calculation of results the bulb was supported from underneath and the first of the two formulas used. The density of the glass was measured and the thickness of the film determined by an optical method. Because of the fact that thin films were used there was a possibility of considerable error in the measurement of the thickness of the film when in the shape of a sphere. However, by making comparison measurements on plane glass films, the maximum possible error in determining the weight of the upper half of the bulb was found not to affect the final results by more than 1.5 percent.

RESULTS

The approximate chemical compositions and densities of some of the glasses tested are given in Table I. In order to show the relationship between temperature, gauge and bulb readings, these quantities are plotted as a function of time for one of the glasses in Fig. 2. Similar curves not reproduced show in many cases less fluctuation

TABLE I. *Composition of glasses investigated.*

	No. 3 Soda-Potash-Lead	No. 4 Potash-Lead	No. 6 Potash-Lead	No. 7 Boro-Silicate	No. 8 Soda-Lime-Zinc	No. 10 Boro-Silicate
SiO_2	62.5	57.5	63.0	81.0	67.0	(Flint?)
PbO	21.0	28.6	22.0	—	—	Alkali-free
Fe_2O_3	0.2	0.2	—	—	—	
Al_2O_3	0.8	1.4	1.0	2.0	2.5	Composition undetermined
CaO	0.5	0.4	—	—	7.0	
MgO	0.5	0.4	—	—	—	
K_2O	6.0	8.0	6.0	—	—	
Na_2O	9.0	4.2	8.0	4.25	14.0	
B_2O_3	—	—	—	12.5	2.0	
ZnO	—	—	—	—	7.0	
Density g/cc	3.34	3.50	3.21	2.28	2.66	2.82

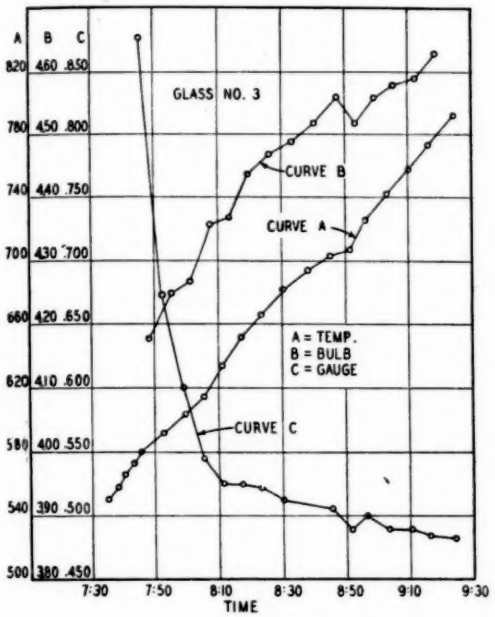

FIG. 2. Curves showing typical relation between the time, temperature (°C), bulb diameter (in cm) and gauge pressures (in cm of water).

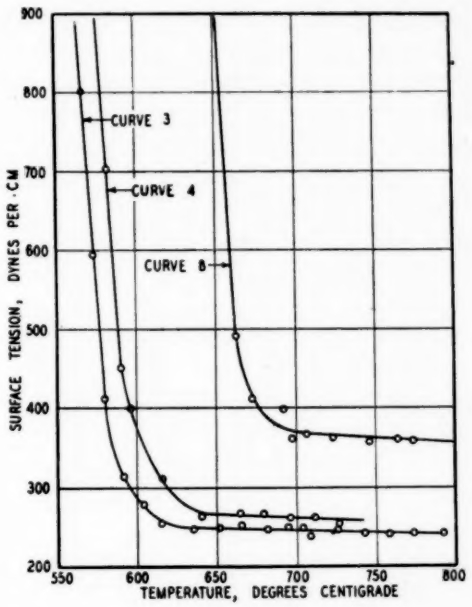

FIG. 3. Variation of surface tension with temperature for the glasses listed in Table I.

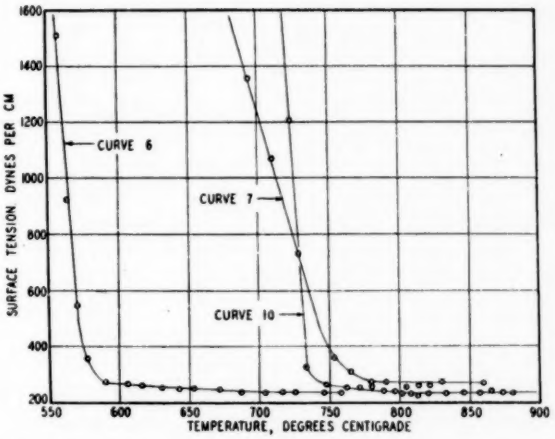

FIG. 4. Variation of surface tension with temperature for the glasses listed in Table I.

in the gauge and bulb readings. The surface tension-temperature data are plotted in Figs. 3 and 4.

The surface tension-temperature curve consists essentially of two parts; a descending branch corresponding to the range of temperature where softening of the glass takes place, and a more nearly horizontal portion extending over the higher range of temperature. It was found that the slope of the descending branch could be changed by changing the rate of heating. This indicates that the softening of the glass is a process that takes place at a fairly definite range of temperature and that requires a certain length of time for its accomplishment. If the furnace is heated rapidly, time is not given for softening to take place in the normal range, but it is spread over a wider range of temperature, thus decreasing the slope of the descending branch of the curve. The rate of heating in the different tests was made as nearly uniform as possible so that the various results would be comparable. This portion of the curve gives very definite informa-

tion concerning the softening temperatures of the different kinds of glasses. It is, however, quite obvious that the high values shown in the curves at low temperatures cannot be interpreted as indicating the true values of surface tension. Here the rigidity or high viscosity of the glass may be such as to mask very largely the effect of the force of surface tension. The values are plotted to indicate only the temperature range where softening of the glass takes place, the true values of surface tension being given over a range of temperature represented by the approximately horizontal portions of the curves. The range of temperature to which the method is applicable will differ for hard and soft glasses as is adequately shown by the curves.

The effect of viscosity in the bulb method of determining surface tension, even at higher temperatures, is a matter which needs to be given careful consideration. If the bulb is expanding when readings are taken the presence of viscous forces would make the calculated values of surface tension too large. In order to obtain the true value of the surface tension of the glass at a definite temperature, obviously the desirable experimental conditions which should be established are such as to keep the temperature, bulb and gauge readings constant. There would then be equilibrium between the forces of surface tension and gas pressure and viscous forces would play no part. Such conditions may be brought about for varying values of temperature and no viscosity correction would need to be made. However, the life of a soft glass bubble is limited and to obtain values of surface tension over a considerable range of temperature a number of glass bulbs might need to be constructed and inserted in the apparatus.

In the determinations of the above results the temperature of the furnace was increased at a nearly uniform rate as shown by the temperature curve of Fig. 2. The average radial velocity of expansion of the bubble was then calculated between successive bulb readings and the results plotted against temperature on the same graph with the calculated surface tension, as illustrated in Fig. 5. Referring to this figure, we see that there is a distinct correlation between the velocity and the calculated surface tension, indicating that the viscosity is producing a noticeable effect.

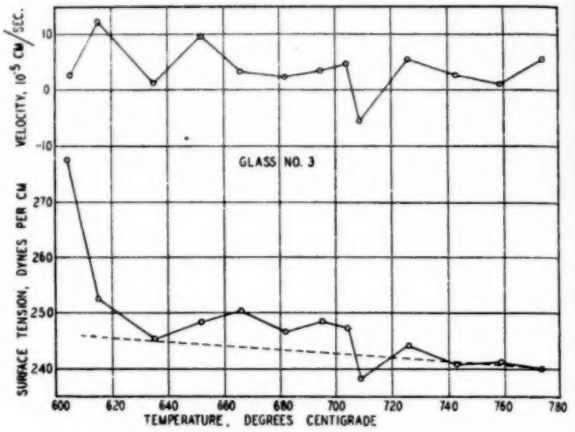

FIG. 5. Surface tension and radial velocity of bulb *vs.* temperature.

The dotted line in Fig. 5 drawn through points where the rate of change of the size of the bulb is practically zero, may be assumed to approximate the true surface tension curve in the temperature range 635°–774° and since the maximum deviation from this line is only about three percent, it is evident that the viscosity correction is practically negligible in this temperature range. Similar results were obtained with the other glasses investigated. It is thus evident that with proper precautions the bulb method is well adapted to the determination of surface tension over a certain temperature range characteristic to the given glass, and the definitely noticeable effect of viscosity makes the method appear a promising one for the determination of viscosity as well. Plans for an experiment of this nature are under way at the University of Colorado.

While in some cases the values of surface tension over the higher portion of the temperature range investigated show no marked tendency to change with temperature, there is in many cases a definite decrease in the values of surface tension with increasing temperature. Assuming that the true surface tension is given approximately by the dotted line in Fig. 5, it is found that between temperatures 635° and 774°C the temperature coefficient for glass 3 is 0.040 dyne per cm per degree C. This is in fairly good agreement with the value of 0.061 found by Washburn and Libman between the temperature of 1206° and 1454°C. Their values of surface tension, however, for this range vary from 128 to 167 dynes per cm

depending upon the temperature and composition of the glass. The results of the present investigation are of the order of 230 to 360 dynes per cm depending upon the kind of glass. These values are approximately midway between those of the two groups of experimenters previously mentioned.

The writer was assisted in the above work by his former student, Mr. H. H. Scott, whose untimely death occurred on July 9, 1934. He acknowledges with sincere appreciation the valuable assistance given him by Mr. Scott in carrying out the experimental work.

Bending of a Centrally Loaded Rectangular Strip of Plywood[1]

H. W. MARCH, *University of Wisconsin*

(Received May 22, 1935)

The deflection of a strip of plywood is calculated for the case in which the load is concentrated along a line through the center of the strip and perpendicular to its edges. This type of loading is commonly used in tests to determine the effective modulus of elasticity in bending. Use is made of the differential equation for a flat plate of plywood. Explicit expressions in terms of the elastic constants of the component plies are given for the coefficients that occur in this equation. For the smaller span-depth ratios the flat plate theory does not lead to exact results. A method is given for calculating the appropriate correction to the results obtained on the basis of this theory.

KNOWLEDGE of the moduli of elasticity in bending in two principal mutually perpendicular planes is necessary for the calculation of the elastic behavior of a flat plate of plywood in a given situation. These moduli are conveniently determined by measuring the deflection of centrally loaded strips simply supported at the ends. In the usual method of testing, the load is applied uniformly across the width of the strip at the center by means of a loading block having on its lower side a cylindrical surface with its elements transverse to the span.

The load may be considered with sufficient approximation to be concentrated uniformly along a line that passes through the center of the strip and is perpendicular to the free edges. From the known load and accompanying deflection it is desired to calculate the effective modulus of elasticity in bending of the strip of plywood composed of layers in which the grain of the wood in one layer is perpendicular to that in adjacent layers with consequent variation of elastic constants with respect to the longitudinal and transverse directions from layer to layer. In this calculation the simple formula $w=Pa^3/48EI$ for the deflection of a centrally loaded beam may be used as a first approximation. In this formula w denotes the deflection at the center, P the load, a the span, E the effective longitudinal modulus of elasticity, and I the moment of inertia of the section of the beam with respect to the neutral axis. Since the thickness of the strips contemplated is small in comparison with the width, they are to be considered as flat plates rather than as beams. It is therefore necessary to examine the correction that is to be made to the foregoing formula to take into account the effect of the anticlastic curvature of a plate subjected to bending moments, this curvature being associated with the transverse contraction or extension accompanying a longitudinal tension or compression, respectively. This correction is found by treating the strip as a thin plate simply supported on two opposite edges and free on the other two edges. To this end the appropriate differential equation is set up for the deflection of a plate of plywood of a given structure under any load normal to its face. This equation is then solved for the type of loading and with the edge conditions as stated above. It is found that the correction for anticlastic curvature is small.

A further correction is necessary to take into account the effect of shear deformation due to shearing stresses in planes perpendicular to the surface of the plate, an effect that is neglected in the theory of thin plates. Because of the relatively low moduli of rigidity of wood the effect of shear deformation may be expected to be considerable for certain arrangements of the plies in the plywood strip when the ratio of the length of the strip to its thickness is not sufficiently great. The correction in question is found as a function of the span-depth ratio by treating the strip as a double cantilever in a state of plane strain. The corrections for anticlastic curvature and for shear deformation are combined as if they were independent in the final formula for the deflection as a function of the load, each correction normally being small.

[1] This investigation was supported by the Wisconsin Alumni Research Foundation. The writer also wishes to acknowledge the extensive cooperation of the U. S. Forest Products Laboratory, maintained at Madison, Wisconsin in cooperation with the University of Wisconsin.

The Differential Equation for the Deflection of a Plywood Plate

In deriving the differential equation for the deflection of a plywood plate the usual assumptions underlying the theory of thin plates are made. In addition the following assumptions are made concerning the elastic behavior of wood and the structure of the plywood.

1. Wood has three mutually perpendicular planes of elastic symmetry.[2]

2. The material of the individual plies is accurately flat-sawn, i.e., the directions of the grain and of the annual rings are parallel to the faces of the plies. The directions of the grain in adjacent plies are perpendicular to each other and parallel or perpendicular to the respective edges of the plate.

3. Each ply is homogeneous. This implies that the variations of the elastic constants from spring wood to summer wood are disregarded and average values of the constants are used.

4. The plate is symmetrical, both geometrically and as to arrangement and properties of the material, with respect to the plane $z=0$, the axes of coordinates being chosen as in Fig. 1.

5. The elastic constants of the wood are the same in all plies. This assumption can be omitted without materially complicating the discussion, provided that the other assumptions are retained.

Under the assumptions made, the components of displacement, parallel to the X and Y axes, respectively, of a point whose coordinate with respect to the middle plane is z, are

$$u=-z\partial w/\partial x, \quad v=-z\partial w/\partial y, \tag{1}$$

where w denotes the deflection.

For a given ply the stress-components in that ply are connected with the strain components, e_{xx}, e_{yy}, e_{xy}, the stress-component Z_z being zero under the assumptions of the thin plate theory, by the relations

$$X_x=\frac{E_x}{1-\sigma_{xy}\sigma_{yx}}(e_{xx}+\sigma_{yx}e_{yy}), \quad X_y=\mu_{xy}e_{xy},$$
$$Y_y=\frac{E_y}{1-\sigma_{xy}\sigma_{yx}}(e_{yy}+\sigma_{xy}e_{xx}), \tag{2}$$

[2] See e.g.: Aeronautics Research Committee (British). Report on the Materials of Construction Used in Aircraft (London, 1920), pp. 95–106. H. Carrington, Phil. Mag. **41**, 206, 848 (1921); **43**, 871 (1922); **44**, 288 (1922); **45**, 105 (1923). A. T. Price, Phil. Trans. **A228**, 1 (1928). H. Hörig, Zeits. f. tech. Physik **12**, 369 (1931).

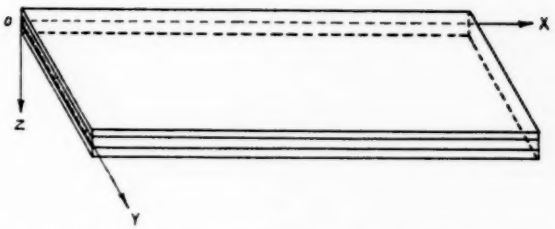

Fig. 1. Orientation of plywood strip with respect to coordinates.

where E_x and E_y are Young's moduli in the directions x and y, respectively, for the ply under consideration, σ_{xy} is the Poisson's ratio associated with contraction parallel to the Y axis and stress parallel to the X axis, and μ_{xy} is the modulus of rigidity corresponding with the directions x and y.[3]

On entering in (2) the components of strain as calculated from (1), the conditions of equilibrium[4] of an element of the plate lead to the following differential equation:

$$D_1\frac{\partial^4 w}{\partial x^4}+2K\frac{\partial^4 w}{\partial x^2\partial y^2}+D_2\frac{\partial^4 w}{\partial y^4}=p, \tag{3}$$

where

$$D_1=\int_{-h/2}^{h/2}E_x z^2dz/(1-\sigma_{xy}\sigma_{yx}),$$
$$D_2=\int_{-h/2}^{h/2}E_y z^2dz/(1-\sigma_{xy}\sigma_{yx}), \tag{4}$$

$$K=\int_{-h/2}^{h/2}\sigma_{yx}E_x z^2dz/(1-\sigma_{xy}\sigma_{yx})+2\int_{-h/2}^{h/2}\mu_{xy}z^2dz, \tag{5}$$

and p is the load per unit area, acting normal to the face $z=-h/2$ in the direction of the positive axis of z.

In obtaining the expression for K the relation[5]

$$\sigma_{xy}E_y=\sigma_{yx}E_x \tag{6}$$

[3] The relations (2) are readily obtained by starting from the expression for the strain-energy function for material having the properties of symmetry that have been assumed. See, for example, A. E. H. Love, *The Mathematical Theory of Elasticity*, Art. 110. See also St. Venant in his annotated translation of Clebsch, *Théorie de l'Elasticité des Corps Solides*, pp. 76–80.

[4] Love, reference 3, Arts. 296, 298, and 313; A. Nadai, Elastische Platten, Art. 10.

[5] See e.g., St. Venant, Annotated Clebsch, p. 80.

has been used. From the expressions given below it can be shown that the coefficients in (3) satisfy the inequality

$$D_1D_2>K^2$$

for a plywood plate; in the case of an isotropic plate $D_1=D_2=K$ and (3) reduces to the well-known equation for isotropic flat plates.

The coefficients occurring in (3) will be expressed in terms of the elastic constants of the wood used, for plywood of the type under consideration. Plies for which the grain is parallel to the axis of X will be referred to as longitudinal plies and those for which the grain is parallel to the axis of Y as transverse plies. Then for longitudinal plies

$$E_x=E_L,\ E_y=E_T,\ \sigma_{xy}=\sigma_{LT},\ \sigma_{yz}=\sigma_{TL},\ \mu_{xy}=\mu_{LT},$$

while for transverse plies

$$E_x=E_T,\quad E_y=E_L,\quad \sigma_{xy}=\sigma_{TL},\quad \sigma_{yz}=\sigma_{LT},$$

$$\mu_{xy}=\mu_{TL}=\mu_{LT}.$$

The subscripts L and T refer to the longitudinal and tangential directions in the wood.

Accordingly, under the assumptions made as to the structure of the plywood, we may write

$$D_1=\frac{E_1h^3}{12(1-\sigma_{LT}\sigma_{TL})}, \tag{7}$$

where

$$E_1=\frac{12}{h^3}\int_{-h/2}^{h/2}E_xz^2dz. \tag{8}$$

The quantity E_1 may be called the apparent Young's modulus in bending[6] in the plane XZ.

In like manner

$$D_2=\frac{E_2h^3}{12(1-\sigma_{LT}\sigma_{TL})}, \tag{9}$$

where E_2 is the apparent modulus in bending in the plane YZ. Its value is obtained by replacing E_x in (8) by E_y.

Further,

$$K=\left(\frac{E_L\sigma_{TL}}{1-\sigma_{LT}\sigma_{TL}}+2\mu_{LT}\right)\frac{h^3}{12}. \tag{10}$$

[6] This term appears to have been introduced by A. T. Price, reference 2.

Boundary Conditions

On the simply supported edges $x=0$, $x=a$ of the rectangular strip to be considered, the deflection w and the flexural couple vanish. Hence on these edges

$$w=0;\quad \partial^2w/\partial x^2+\sigma_1\partial^2w/\partial y^2=0; \tag{11}$$

where

$$\sigma_1=E_L\sigma_{TL}/E_1. \tag{12}$$

On the free edges $y=0$ and $y=b$ the flexural couple and the transverse shear per unit length of edge,[7] $N_2+\partial H_2/\partial x$ vanish. Hence on these edges

$$\begin{aligned}\partial^2w/dy^2+\sigma_2\partial^2w/dx^2=0;\\ d^3w/\partial y^3+(2-\sigma)\partial^3w/\partial x^2\partial y=0;\end{aligned} \tag{13}$$

where

$$\sigma_2=E_L\sigma_{TL}/E_2, \tag{14}$$

and

$$\sigma=[(2-\sigma_2)E_2-4\mu_{LT}(1-\sigma_{LT}\sigma_{TL})]/E_2. \tag{15}$$

Rectangular Strip of Plywood

A rectangular strip of plywood is simply supported at its ends, $x=0$ and $x=a$, and supports a concentrated load P acting uniformly on the central line $x=a/2$. The edges, $y=0$ and $y=b$, of the strip are free. The intensity of the load per unit length of the central line is P/b. At all points except those on the line $x=a/2$ the deflection satisfies the differential Eq. (3) with $p=0$. The vertical component of shearing force per unit length N_1 is discontinuous across the line $x=a/2$, the magnitude of the discontinuity being P/b.

Now

$$N_1=-D_1\partial^3w/\partial x^3-K\partial^3w/\partial x^2\partial y^2. \tag{16}$$

The discontinuity in N_1 is then expressed by

$$\left[D_1\frac{\partial^3w}{\partial x^3}+K\frac{\partial^3w}{\partial x\partial y^2}\right]_{x=a/2+0}-\left[D_1\frac{\partial^3w}{\partial x^3}+K\frac{\partial^3w}{\partial x\partial y^2}\right]_{x=a/2-0}=P/b. \tag{17}$$

[7] Love, reference 3, Art. 297.

Two solutions of Eq. (3) with $p=0$ will be combined to satisfy the boundary conditions (11) and (13) together with the condition of discontinuity in shear (17) at the transverse central line. One of these which may be expected to be a fair approximation to the final solution is suggested by the deflection of a simple beam loaded at its center and simply supported at its ends, *viz.*,

$$w_1=A(3a^2x-4x^3), \quad x<a/2$$
$$=A[3a^2(a-x)-4(a-x)^3], \quad x>a/2. \quad (18)$$

In order that (17) may be satisfied A must have the value

$$A=\frac{P}{48D_1b}=\frac{P(1-\sigma_{LT}\sigma_{TL})}{48E_1I},$$

where $I=bh^3/12$.

The solution (18) of (3) with $p=0$ does not satisfy the boundary conditions (13) of zero shear and zero bending moment on the two free edges of the strip. Edge bending moments and shears must act to bend the strip from its natural state of anticlastic curvature into the cylindrical surface w_1. A solution w_2 of (3) with $p=0$ must be added to the solution w_1, which will yield bending moments and shearing forces on the edges $y=0$ and $y=b$ that will exactly balance those yielded by w_1 and render these edges free from external forces. As such a solution choose

$$w_2=\sum A_nY_n(y)\sin\lambda_nx, \quad \lambda_n=n\pi/a, \quad (19)$$

where Y_n satisfies the equation

$$D_2\frac{d^4Y_n}{dy^4}-2K\lambda_n^2\frac{d^2Y_n}{dy^2}+D_1\lambda_n^4Y_n=0.$$

The function w_2 satisfies the differential Eq. (3) with $p=0$ and the boundary conditions (11) on the supported edges $x=0$ and $x=a$.

The usual method of solving the ordinary linear differential equation for Y_n leads to a linear combination of four products of one trigonometric and one hyperbolic function of y each. The constants that enter in this linear combination are to be chosen in such a way that the sum w_1+w_2 satisfies the conditions (13). It is thus found that the deflection $w=w_1+w_2$ at any point is given by

$$w=\frac{P(1-\sigma_{LT}\sigma_{TL})}{48E_1I}\left\{3a^2x-4x^3\right.$$
$$\left.+\frac{96\sigma_2a^3}{\pi^4}\sum\frac{(-1)^{(n-1)/2}}{n^4}\frac{\begin{array}{r}\sin\delta_n(y-b)\cosh\gamma_ny-\sin\delta_ny\cosh\gamma_n(y-b)\\+\epsilon[\cos\delta_n(y-b)\sinh\gamma_ny-\cos\delta_ny\sinh\gamma_n(y-b)]\end{array}}{M\sin\delta_nb+N\cos\delta_nb}\cdot\sin\lambda_nx\right\}, \quad (20)$$
$$n=1, 3, 5, \cdots, \quad x\leqq a/2.$$

If $x\geqq a/2$, the polynomial in (20) is to be replaced by $3a^2(a-x)-4(a-x)^3$.

In (20) the constants have the following meanings:

$$\delta_n=\frac{\lambda_n}{(2D_2)^{\frac{1}{2}}}((D_1D_2)^{\frac{1}{2}}-K)^{\frac{1}{2}},$$
$$\gamma_n=\frac{\lambda_n}{(2D_2)^{\frac{1}{2}}}((D_1D_2)^{\frac{1}{2}}+K)^{\frac{1}{2}}, \quad (21)$$
$$\epsilon=\frac{\delta_n(D_1D_2)^{\frac{1}{2}}+2K-D_2(2-\sigma)}{\gamma_n(D_1D_2)^{\frac{1}{2}}-2K+D_2(2-\sigma)}$$
$$=-\frac{\delta_n(E_1E_2)^{\frac{1}{2}}+E_L\sigma_{TL}}{\gamma_n(E_1E_2)^{\frac{1}{2}}-E_L\sigma_{TL}}, \quad (22)$$

$$M=[\sigma_2D_2-K+\epsilon(D_1D_2-K^2)^{\frac{1}{2}}]/D_2, \quad (23)$$
$$N=[\epsilon(K-\sigma_2D_2)+(D_1D_2-K^2)^{\frac{1}{2}}]/D_2. \quad (24)$$

From (20) the deflection at points on the central line $x=a/2$ is given by

$$w=\frac{P(1-\sigma_{LT}\sigma_{TL})a^3}{48E_1I}B, \quad (25)$$

where B is a function of y.

The quantity B was calculated at the center and ends of the line of loading for strips of spruce plywood. The elastic constants were

taken[8] to be:

$$E_L=1.95\times10^6 \text{ lb./in.}^2, \quad \sigma_{LT}=0.539,$$
$$E_T=0.07\times10^6 \text{ lb./in.}^2, \quad \sigma_{TL}=0.019,$$
$$\mu_{LT}=0.072\times10^6 \text{ lb./in.}^2.$$

It will be assumed from this point on, for simplicity, that all plies are of the same thickness.

The apparent moduli in bending E_1 and E_2 that are needed were calculated for three-ply, five-ply, seven-ply and nine-ply strips. The following formulas, in which

$$r=E_T/E_L, \tag{26}$$

can be readily found by applying (8) to the type of plywood under consideration. The outer plies were taken to be longitudinal.

$$\text{Three-ply, } E_1=\frac{r+26}{27}E_L, \qquad E_2=\frac{1+26r}{27}E_L,$$

$$\text{Five-ply, } E_1=\frac{26r+99}{125}E_L, \qquad E_2=\frac{26+99r}{125}E_L, \tag{27}$$

$$\text{Seven-ply, } E_1=\frac{99r+244}{343}E_L, \qquad E_2=\frac{99+244r}{343}E_L,$$

$$\text{Nine-ply, } E_1=\frac{244r+485}{729}E_L, \quad E_2=\frac{244+485r}{729}E_L.$$

If the outer plies are transverse, E_1 and E_2 above are to be interchanged.

With the elastic constants for spruce, the values for E_1 and E_2 in Table I were found, the outer plies being taken to be longitudinal.

The quantity B and $(1-\sigma_{LT}\sigma_{TL})B$ were found to have the values given in Table II, at the points $x=a/2$, $y=b/2$ and $x=a/2$, $y=b$.

For strips of three plies with the outer plies transverse the number $(1-\sigma_{LT}\sigma_{TL})B$ differs from 0.995 by 0.001 or less for both $y=b/2$ and $y=b$ for the ratios a/b considered and for strips of five plies with the outer plies transverse the same number differs from 0.992 by 0.001 or less.

TABLE I. *Apparent moduli in bending of spruce plywood.*

NUMBER OF PLIES	E_1/E_L	E_2/E_L
3	0.964	0.072
5	0.799	0.236
7	0.722	0.314
9	0.678	0.359

TABLE II. *Values of the factor B.*

a/b	$B(y=b/2)$	$B(y=b)$	$(1-\sigma_{LT}\sigma_{TL})B$ $y=b/2$	$(1-\sigma_{LT}\sigma_{TL})B$ $y=b$
	Three plies—Outer plies longitudinal			
4	0.9987	1.0171	0.9884	1.0067
8	1.0033	1.0086	0.9931	0.9983
12	1.0044	1.0068	0.9941	0.9965
	Five plies—Outer plies longitudinal			
4	0.9998	1.0061	0.9895	0.9958
8	1.0013	1.0030	0.9911	0.9927
12	1.0017	1.0024	0.9914	0.9921

The factor $(1-\sigma_{LT}\sigma_{TL})B$ occurring in (25) is the factor by which the deflection as given by the simple formula for beams is to be multiplied to correct for the effect of anticlastic curvature. Table II shows that this correction is small, being approximately one percent. Furthermore, the small difference between the deflections on the transverse central line at the center and the edge of the plate, as given in the fourth and fifth columns of Table II, shows that no appreciable error can result from the fact that the load is actually applied by a rigid loading block and is not the ideally uniform loading along the transverse central line as assumed in the analysis.

Under the same type of loading and the same boundary conditions as above the deflection of a rectangular strip of isotropic material is readily found by the method previously used, to be given by

$$w=\frac{P(1-\sigma^2)}{48EI}\left\{3a^2x-4x^3+\frac{96\sigma}{a}\sum_n(-1)^{(n-1)/2}\frac{1}{\lambda_n^3[(3+\sigma)\sinh\lambda_nb-(1-\sigma)\lambda_nb]}\right.$$
$$\cdot[(y-b)\cosh\lambda_ny-y\cosh\lambda_n(y-b)$$
$$\left.+\frac{1+\sigma}{(1-\sigma)\lambda_n}(\sinh\lambda_ny-\sinh\lambda_n(y-b))]\sin\lambda_nx\right\}, \quad n=1, 3, 5, \cdots \tag{28}$$

[8] C. F. Jenkin, Report on Materials of Construction Used in Aircraft, Aeronautical Research Committee (British) (1920), p. 105.

when $x \leqq a/2$. When $x \geqq a/2$ the polynomial in x is to be replaced by $3a^2(a-x)-4(a-x)^3$. In (28) σ denotes Poisson's ratio.

At points on the transverse central line the deflection is given by

$$w=\frac{P(1-\sigma^2)a^3}{48EI}B, \qquad (29)$$

where B is a function of y.

Table III gives the value of B and of $(1-\sigma^2)B$

TABLE III. *Values of the factor B in Eq. (29).*

a/b	$B(y=b/2)$	$B(y=b)$	$(1-\sigma^2)B$ $y=b/2$	$(1-\sigma^2)B$ $y=b$
1	1.0119	1.1825	0.8995	1.0511
2	1.0690	1.1527	0.9502	1.0246
4	1.1063	1.1339	0.9834	1.0079
8	1.1209	1.1272	0.9964	1.0020
12	1.1224	1.1259	0.9977	1.0008
16	1.1234	1.1254	0.9986	1.0004
24	1.1241	1.1250	0.9992	1.0000

for various ratios of a to b, at two points on the central line $x=a/2$, *viz.*, at $y=b/2$, the center; and at $y=b$, the edge. The value of σ was taken to be 1/3.

Rectangular Strip as a Double Cantilever in a State of Plane Strain

In the foregoing analysis the central deflection of a centrally loaded strip of plywood was found by treating the strip as a thin plate. This amounted essentially to the determination of the correction to the simple formula for a centrally loaded beam to account for the effect of anticlastic curvature. However, the differential equation for the deflection of a thin plate is derived on the assumption that the transverse shearing stresses Z_x, Z_y are negligible in comparison with the stresses parallel to the plane of the plate. This assumption becomes increasingly inaccurate as the ratio of the thickness of the plate to its span increases and a correction to the deflection as calculated above becomes necessary to take into account the effect of the deformation accompanying the shearing stresses that were neglected in the thin plate theory. In extreme cases this correction may be considerable but in normal test specimens it will be found to be less than ten percent. An estimate

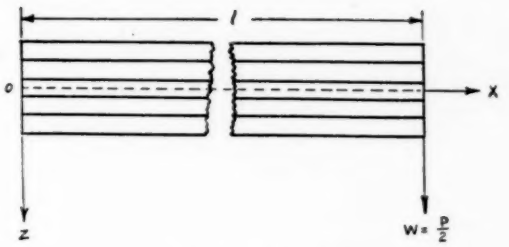

FIG. 2. Dimensions and choice of origin for cantilever.

of the correction which must be applied to formula (25) will be obtained by considering the rectangular strip, loaded as before, as made up of two cantilevers fixed at their junction at the center $x=a/2$ and under the action of a load $P/2$ at the end of each, *viz.*, at $x=0$ and $x=a$. The cantilevers will be taken to be in a state of plane strain.[9]

For purposes of illustrating the method a cantilever of plywood consisting of five plies, and having the outer plies longitudinal, will be considered. The dimensions and choice of origin and axes are shown in Fig. 2.

It will be noted that the fixed end $x=0$ is to correspond to the center $x=a/2$ of the strip previously considered and that the length l is equal to one-half the span a of the strip.

In the state of plane strain it is assumed that the components of displacement u and w are functions of x and z only and that $v=0$. All components of stress and strain are independent of y. The strain components e_{xy}, e_{yz}, e_{yy}, and the stress components X_y, Y_z all vanish. The stress component Y_y is in general not zero. Hence, to maintain the strip in a state of plane strain a tension or pressure must be applied on the faces at the edges $y=0$ and $y=b$.

At the planes of separation of adjacent plies the following conditions hold:[10]

The components of stress Z_z and X_z are continuous.

The components of displacement u and w are continuous.

Within each ply the components of strain and stress are connected by the relations:[11]

[9] Love, reference 3, Art. 94; Nadai, reference 4, Art. 15.
[10] See, for example, Price, reference 2, p. 13.
[11] These relations are readily derived from the strain-energy function given in Eq. (15), Art. 110, Love, for material having three orthogonal planes of elastic symmetry. See also St. Venant, reference 3, p. 80.

$$e_{xx}=\frac{1}{E_x}X_x-\frac{\sigma_{xy}}{E_x}Y_y-\frac{\sigma_{xz}}{E_x}Z_z,$$

$$e_{yy}=-\frac{\sigma_{xy}}{E_x}X_x+\frac{1}{E_y}Y_y-\frac{\sigma_{zy}}{E_z}Z_z, \tag{30}$$

$$e_{zz}=-\frac{\sigma_{xz}}{E_x}X_x-\frac{\sigma_{zy}}{E_z}Y_y+\frac{1}{E_z}Z_z.$$

Since $e_{yy}=0$, it follows that

$$Y_y=\frac{E_y}{E_x}\sigma_{xy}X_x+\frac{E_y}{E_z}\sigma_{zy}Z_z. \tag{31}$$

On substituting this expression for Y_y in the other two equations, it is found after some reduction that

$$e_{xx}=\alpha X_x-\beta Z_z, \quad e_{zz}=-\beta X_x+\gamma Z_z, \tag{32}$$

where

$$\alpha=\frac{1}{E_x}(1-\sigma_{xy}\sigma_{yx}), \quad \beta=\frac{1}{E_z}(\sigma_{xy}\sigma_{yz}+\sigma_{xz}),$$
$$\gamma=\frac{1}{E_z}(1-\sigma_{zy}\sigma_{yz}). \tag{33}$$

Within each ply the equations of equilibrium for the stress components X_x, X_z, Z_z, assure the existence of a stress function F such that

$$X_x=\partial^2F/\partial z^2,\ Z_z=\partial^2F/\partial x^2,\ X_z=-\partial^2F/\partial x\partial z. \tag{34}$$

The condition of compatibility of the strain components leads to the following differential equation for F:

$$\alpha\frac{\partial^4F}{\partial x^4}+\left(\frac{1}{\mu_{xz}}-2\beta\right)\frac{\partial^4F}{\partial x^2\partial z^2}+\gamma\frac{\partial^4F}{\partial z^4}=0. \tag{35}$$

A suitable solution[12] of (35) is given by

$$F=g(x-l)(z^3/3-h^2z/4). \tag{36}$$

Relations of the form expressed by Eqs. (30)–(36) hold for each of the plies separately. It follows that the stress function F is to be chosen differently for each ply. The subscript 1 will be used to denote quantities associated with the center ply, the subscript 2 those associated with the adjacent plies, and no subscript to denote the same quantities associated with the outer plies. It will be necessary to carry out the analysis only for the half of the strip for which z is positive. It will be clear that the expressions thus obtained also apply in the appropriate plies when z is negative. It will be convenient to denote the thickness of a single ply by $2c$.

We write

$$F_1=g_1(x-l)(z^3/3-h_1^2z/4), \quad 0<z<c \tag{37}$$

and analogous expressions for the plies $c<z<3c$ and $3c<z<5c$. The constants that appear are to be determined from the boundary conditions, from the conditions that hold at the surfaces of separation of two adjacent plies, from the condition that

$$\int_{-h/2}^{h/2}X_x\,dz=P/2b \tag{38}$$

and from the condition that

$$X_x=0, \quad z=\pm h/2. \tag{38a}$$

It follows from (37) and (34) that

$$X_x=2g_1(x-l)z, \quad Z_z=0, \quad X_z=g_1(h_1^2/4-z^2) \tag{39}$$

if $0<z<c$, and that corresponding relations containing constants with different subscripts hold in the remaining plies where $c<z<3c$ and $3c<z<5c$, respectively.

The differential equations satisfied by the displacements are obtained from (32) and (39). Thus

$$\partial u_1/\partial x=2\alpha_1g_1(x-l)z,\ \partial w_1/\partial z=-2\beta_1g_1(x-l)z,$$
$$\partial u_1/\partial z+\partial w_1/\partial x=(g_1/\mu_1)(h_1^2/4-z^2). \tag{40}$$

Similar differential equations hold in the remaining plies. Since the direction of the grain in the central ply is the same as that in the outer plies, the constants α_1, β_1, and μ_1 are the same as α, β, and μ for the outer plies. It is to be observed that $\mu_1=\mu=\mu_{xz}=\mu_{LR}$ for the central and outer plies and that $\mu_2=\mu_{xz}=\mu_{TR}$ for the intermediate plies.

Integration of the system (40) leads to the results

[12] See, for example, Nadai, reference 4, p. 49.

$$u_1=\alpha_1 g_1(x-l)^2 z+\beta_1 g_1\frac{z^3}{3}+\frac{g_1}{\mu_1}\left(\frac{h_1^2 z}{4}-\frac{z^3}{3}\right)+k_1 z+m_1,$$
$$w_1=-\beta_1 g_1(x-l)z^2-\alpha_1 g_1\frac{(x-l)^3}{3}-k_1 x+n_1. \tag{41}$$

Expressions for the displacements in the remaining plies are found by changing the subscripts throughout.

The condition of continuity of the components of shearing stress X_z at the planes of separation of adjacent plies leads to expressions for the constants h_1 and h_2 in terms of g, g_2 and h.

From the continuity of the components of displacement u at the planes of separation of adjacent plies, it results that

$$g_2=\lambda g, \quad \text{where} \quad \lambda=\alpha/\alpha_2=E_T/E_L \tag{42}$$

for the arrangement of plies under consideration, *viz.*, longitudinal central and outer plies. It is thus found that

$$\begin{aligned} X_z&=g(\kappa_1 h^2-z^2), \quad 0<z<c,\\ X_z&=g(\kappa_2 h^2-\lambda z^2), \quad c<z<3c,\\ X_z&=g(\kappa h^2-z^2), \quad c<z<5c, \end{aligned} \tag{43}$$

where

$$\kappa_1=0.17+0.08\lambda, \quad \kappa_2=0.16+0.09\lambda, \quad \kappa=0.25. \tag{44}$$

The substitution of the expressions for X_z in (38) leads to

$$g=\tfrac{1}{4}PE_L/E_1 I. \tag{45}$$

The remaining arbitrary constants in the expressions (41) for the displacements are determined from the continuity of the displacements at the planes of separation and from the conditions at the end $x=0$. The latter will be taken to be:

$$\begin{aligned} &u_1=0, \quad x=0, \quad z=0,\\ &u=0, \quad x=0, \quad z=\pm 5c=\pm h/2,\\ &w_1=0, \quad x=0, \quad z=0. \end{aligned} \tag{46}$$

On replacing l by $a/2$ the following expression is found for the deflection w_1 at $x=l=a/2$, $z=0$:

$$w_1=\frac{(1-\sigma_{LT}\sigma_{TL})Pa^3}{48E_1 I}\left[1+e\frac{h^2}{a^2}\right], \tag{47}$$

where

$$e=4\left[0.057\frac{\beta}{\alpha}+0.068\frac{\beta_2\lambda}{\alpha}+\frac{0.102+0.024\lambda}{\alpha\mu}+\frac{0.096+0.028\lambda}{\alpha\mu_2}\right], \tag{48}$$

where $\mu=\mu_{LR}$ and $\mu_2=\mu_{TR}$ if the outer plies are longitudinal.

The expression (47) represents the deflection at the center of a five-ply rectangular strip of plywood treated as a double cantilever in a state of plane strain. This deflection will be compared below with that given by Eq. (25) resulting from treating the strip as a thin plate.

The deflections of three-ply, seven-ply, and nine-ply strips under the same type of central load and with the outer plies longitudinal are found by a similar analysis to be given by (47) where E_1 is to be calculated for the appropriate number of plies by (27) and the constant e has the value given below.

For three-ply strips

$$e=4\left[0.093\frac{\beta}{\alpha}+0.032\frac{\beta_1\lambda}{\alpha}+\frac{0.130}{\alpha\mu}+\frac{0.111+0.0093\lambda}{\alpha\mu_1}\right], \tag{49}$$

where $\mu=\mu_{LR}$, $\mu_1=\mu_{TR}$. The constants α and β are to be calculated for the outer plies and β_1 for the central ply by (33).

For seven-ply strips

$$e=4\left[0.067\frac{\beta}{\alpha}+0.058\frac{\beta_1\lambda}{\alpha}+\frac{0.0904+0.0350\lambda}{\alpha\mu}+\frac{0.0875+0.0371\lambda}{\alpha\mu_1}\right], \tag{50}$$

where $\mu=\mu_{LR}$, $\mu_1=\mu_{TR}$. The constants α and β are to be calculated for the outer plies and β_1 for the central ply by (33).

For nine-ply strips

$$e=4\left[0.060\frac{\beta}{\alpha}+0.064\frac{\beta_2\lambda}{\alpha}+\frac{0.0840+0.0412\lambda}{\alpha\mu}-\frac{0.0823+0.0425\lambda}{\alpha\mu_2}\right], \quad (51)$$

where $\mu=\mu_{LR}$, $\mu_2=\mu_{TR}$. The constants α and β are to be calculated for the outer plies and β_2 for an adjacent ply by (33).

In obtaining (49)–(51) end conditions were used analogous to those used in discussing the five-ply strip. In particular, $u=0$ when $x=0$ and $z=\pm h/2$.

In the analysis leading to Eqs. (47)–(51) it was assumed, in order to have a definite situation in mind, that the outer plies were longitudinal. These equations also hold, with appropriate changes in the quantities involving the elastic constants, for strips of plywood with the outer plies transverse. In particular, it is to be noted that $\lambda=E_L/E_T$ when the outer plies are transverse and that E_1 has the value given for E_2 in Eqs. (27) and that μ_{LR} and μ_{TR} are to be interchanged.

The deflection of a flat sawn strip of wood, *viz.*, a single ply having the grain longitudinal and the annual rings horizontal, is found under the same conditions to be given by (47) with

$$E_1=E_L \quad \text{and} \quad e=0.5\beta/\alpha+1/\alpha\mu_{LR}, \quad (52)$$

α and β being calculated by (33).

With the elastic constants of spruce, the values in Table IV were calculated for e for strips of three, five, seven, and nine plies, the constant appearing in Eq. (47).

For a flat sawn strip of spruce, $e=19.2$.

The constant e was determined experimentally in a brief series of tests with commercial Douglas Fir plywood of three and five plies. The thickness of the three-ply and five-ply strips was 3/8 in. and 1/2 in. respectively. The tests were made by starting with long strips and shortening them for successive tests by sawing off portions at the ends. The corresponding values of e were calculated by Eqs. (48) and (49) using the values of the elastic constants of Douglas Fir as determined from a small number of tests. A more extensive series of tests is contemplated using plywood more closely approximating the ideal structure assumed in the mathematical analysis. The calculated and observed values of e resulting from the tests already made are given in Table V. The two numbers in the last column correspond to two different strips. The last numbers in the last column were too small to be determined with any degree of accuracy. This could have been anticipated from the small theoretical value of e.

TABLE IV. *Values of e in Eq. (47).*

NUMBER OF PLIES	e (Outer plies longitudinal)	e (Outer plies transverse)
3	184.8	8.6
5	160.8	46.3
7	147.1	63.5
9	138.8	73.3

TABLE V. *Results of tests on Douglas Fir plywood.*

	e CALCULATED	e OBSERVED
5 Plies—Outer plies longitudinal	118.4	90–100
5 Plies—Outer plies transverse	36.6	36– 37
3 Plies—Outer plies longitudinal	141.7	112–132
3 Plies—Outer plies transverse	9.8	—

For a flat sawn solid beam of Douglas Fir the constant e as calculated by (52) is found to be 19.6. while values calculated from tests made by Newlin and Trayer[13] on such beams range from 16 to 21.

Taking into consideration the possible variation in the elastic constants of the wood and the deviation in the case of the plywood from the assumed ideal structure, the agreement between the calculated and observed values of e is regarded as satisfactory.

The values of e in Table IV reflect the influence of the extremely low modulus of rigidity μ_{RT}, the "modulus of rolling shear" that is effective in the transverse plies. In such plies the shearing strains are relatively very large. This influence is particularly noticeable in the case of a three-ply strip that has the outer plies longitudinal. There is a relatively large distortion due to shear in the transverse central ply where the shearing stress is a maximum. To this situation is to be attributed the large value of e, *viz.*, $e=184.8$. On the other hand, when the outer plies are transverse the low modulus of rolling shear μ_{RT} is

[13] J. A. Newlin and G. W. Trayer, "Deflection of Beams with Special Reference to Shear Deformations," National Advisory Committee for Aeronautics, Ninth Annual Report, pp. 357–373.

effective in regions where the shearing stress is low, while the modulus μ_{LR} that is about twenty times μ_{RT} is effective in the central ply where the shearing stress is high. Hence, the value of e found for this case, *viz.*, $e=8.6$, is relatively small.

The magnitude of the effect of shear deformation may be shown by calculating the value of the factor, $1+eh^2/a^2$, for two strips of definite dimensions. Thus for a three-ply strip of spruce plywood 3/8 in. thick and 16 in. long and having the face plies longitudinal, it is found that $1+eh^2/a^2=1.10$. For a five-ply strip 0.5 in. thick and 24 in. long and having the face plies longitudinal the same factor has the value 1.07. The effect in these cases is appreciable and would have to be taken into consideration in evaluating tests made with specimens of these dimensions, for the determination of the effective modulus of elasticity in bending.

In Eq. (47) the correction to be made for shear deformation is shown by the factor $1+eh^2/a^2$. This correction will be combined with that for the effect of anticlastic curvature as expressed in formula (25) by introducing the factor $1+eh^2/a^2$ in the right-hand member of Eq. (25), thus combining the two corrections as if they were independent. Accordingly the formula for the central deflection, taking into account the effects of anticlastic curvature and shear deformation, becomes

$$w=(Pa^3/48E_1I)(1-\sigma_{LT}\sigma_{TL})B(1+eh^2/a^2). \quad (53)$$

Since the value of the quantity $(1-\sigma_{LT}\sigma_{TL})B$ differs but little from unity for moderately long strips, e.g., $a/b>8$, as was shown in Table II, it follows that the central deflection for such strips is given approximately by the simple theory of beams if the effect of shear deformation is adequately taken into account.